THE ASTROPHYSICAL JOURNAL, 330:964–985, 1988 July 15

DIFFUSE INFRARED EMISSION FROM THE GALAXY. I. SOLAR NEIGHBORHOOD

F. BOULANGER
Infrared Processing and Analysis Center, California Institute of Technology; Ecole Normale Supérieure, Paris
AND
M. PÉRAULT
Ecole Normale Supérieure, Paris
Received 1987 June 29; accepted 1987 December 30

ABSTRACT

A large-scale study of the infrared emission originating in the solar neighborhood, based on the analysis of *IRAS* data, is presented. Basic properties of the infrared emission from the interstellar medium are derived from this study.

Away from heating sources and outside molecular clouds the infrared emission from the interstellar medium is well correlated with the column density of H I gas. This correlation proves that the interstellar radiation field and the dust abundance are roughly uniform on scales of the order of 100 pc. Dust in molecular clouds not associated with H II regions is heated by the external radiation field; on average, embedded stars have a negligible contribution to their IR emission; these clouds have an infrared-luminosity–to–mass-of-gas ratio of 0.6 $L_\odot/M_\odot$, about one-third of the value measured for atomic gas. Away from internal sources of heating the 100 μm emission from molecular clouds is correlated with the column density of gas up to A_v of ~ 3 mag. The infrared emission from H II regions and diffuse ionized gas is also analyzed. Results of the correlation between infrared emission and gas column density are used to discuss the extinction in the polar caps.

The origin of the infrared emission from the solar neighborhood is investigated. We show that stars younger than a few 10^8 yr are responsible for two-thirds of the infrared emission from the solar neighborhood, but that most of this emission comes from interstellar matter not associated with current star formation. A study of the Orion region emphasizes this result by showing that only a small fraction of the luminosity of an OB association is locally converted into infrared radiation.

By comparing the distribution of infrared and radio-continuum emission around Orion we show that the correlation between infrared and radio-continuum fluxes of galaxies breaks down on the scale of a few hundred parsecs around regions of star formation, which implies that the relationship between infrared and radio fluxes seen in external galaxies originates on a larger scale.

We show the existence of 12 and 25 μm emission from the Galaxy at $|b| > 10°$, and demonstrate that this emission comes from dust heated by the average interstellar radiation field of the Galaxy; we find that the emission between 7 and 35 μm represents $\sim 40\%$ of the power radiated at $\lambda < 120$ μm. This result proves the pervasive existence of grains small enough to be heated to a few 100 K when they absorb a single photon.

After subtraction of the zodiacal light and the Galactic emission we find at 100 μm a residual background in the range 1.2–1.8 MJy sr^{-1}; we suggest several explanations for this emission.

Subject headings: infrared: general — interstellar: grains — interstellar: matter — interstellar: molecules

I. INTRODUCTION

By providing the first extensive set of data on the infrared emission originating in the solar neighborhood, the *Infrared Astronomy Satellite* (*IRAS*) has opened the way to new studies of interstellar matter. The sensitivity of *IRAS* observations was sufficient to detect emission from clouds with column densities as low as a few 10^{19} H atoms cm^{-2} (Boulanger, Baud, and van Albada 1985). With such a sensitivity, *IRAS* observations may be used to probe the spatial distribution of dust and gas and to study the properties of dust grains in the different phases of the interstellar medium.

Within a few kiloparsecs from the Sun the different components of the interstellar medium—neutral atomic gas, molecular clouds, and H II regions—can be observed and studied separately. For each of these components we can identify the heating source of the dust and understand the origin of the infrared emission because we know the interstellar radiation field and the distribution of stars. The detailed analysis of the infrared emission from the interstellar medium which can be done in the solar neighborhood can answer fundamental questions about the infrared emission of the Galaxy and external galaxies—for example, the contribution of young stars to the heating of dust, the origin of the mid-infrared emission, and the nature of the correlation between infrared and radio-continuum emission (Puget 1985; Pajot *et al.* 1986; Ghosh, Drapatz, and Peppel 1986; de Jong *et al.* 1985; Helou, Soifer, and Rowan-Robinson 1985).

In this paper, basic properties of the infrared emission of the different components of the interstellar medium within 1 kpc of the Sun are derived from a large-scale comparison of infrared, H I, CO, and radio-continuum observations. Subsequently, these properties are used to discuss the origin of the infrared emission from the solar neighborhood and dust properties. The extension of this study to the inner parts of the Galaxy is presented in a second paper, Pérault *et al.* (1987, hereafter Paper II).

The observations used in this investigation are described in § II. Section III is focused on the infrared emission from H I and diffuse ionized gas. A study of the infrared emission of molecular clouds is presented in § IV. We discuss the emission of H II regions in § V. The results of the three preceding sections are used in § VI to discuss the origin of the infrared emission on the scale of the whole solar neighborhood and individual star-forming regions. In § VII we show that the correlation between infrared and radio-continuum emission seen in galaxies breaks on the scale of a few hundred parsecs around star-forming regions. The observations presented in this paper provide informations on interstellar dust which are discussed in § VIII. The main results of the paper are summarized in § IX. The paper has three appendices. Appendix A describes the subtraction of the zodiacal light; the question of the existence of a residual background at 100 μm is addressed in Appendix B; Appendix C summarizes data on the OB association and the interstellar medium in the Orion region.

II. PRESENTATION OF DATA

Our investigation is based on a large-scale comparison of *IRAS* observations outside the Galactic plane with H I, CO and radio-continuum data. The data used in these investigations are presented in this section.

a) Infrared Data

All-sky maps of the Galactic emission at 12, 25, 60, and 100 μm were built from the zodiacal history file, a 0°.5 resolution, time-ordered data set containing all three sky coverages of the *IRAS* survey (*IRAS Explanatory Supplement 1985*, hereafter the Supplement). The subtraction of the zodiacal light was done on a scan-by-scan basis before the projection of the data onto an all-sky grid (Appendix A). When a resolution better than 0°.5 was needed, we used sky brightness images sampled every 2′ built from the *IRAS* survey observations (Sky Flux Images, see the Supplement).

Uncertainties on the absolute photometric calibration of *IRAS* observations are estimated to be of the order of 5% at 12 and 25 μm, and 20% at 60 and 100 μm (Supplement). The noise in the maps of Galactic emission comes mainly from the subtraction of the zodiacal light; the root mean square dispersion is estimated to 0.1, 0.2, 0.4, and 0.5 MJy sr^{-1} at 12, 25, 60 and 100 μm, respectively (Appendix A). The zero level of the Galactic emission was determined by forcing the intercept of the infrared–H I correlation in the polar caps to be zero (see below, § III*c*, Fig. 5). This determination of the zero level assumes that there is no emission from ionized gas in the holes of H I emission. If the H I holes are not regions of low column density of ionized gas, our reference is above the true zero level of Galactic emission; for an emissivity similar to that for the neutral gas we expect the 100 μm emission from ionized gas to be 0.6 MJy sr^{-1} in average at high latitude (see § III*d*). Results presented outside §§ III*d* and III*f* and Appendix B do not depend on this uncertainty on the zero level of the Galactic emission.

Throughout this paper, the *IRAS* in-band fluxes are expressed as monochromatic flux densities, I_ν, at 12, 25, 60, and 100 μm, under the assumption of a ν^{-1} spectrum within each band. The sum of $4\pi\nu I_\nu$ over the four *IRAS* wavelengths is for the spectrum of the inner Galaxy a good approximation of the infrared emission integrated from 5 μm to 1 mm (Paper II); this sum is used throughout the paper to derive total infrared fluxes from the *IRAS* measurements.

b) H I Data

The surveys of Heiles and Habing (1974), Weaver and Williams (1973), Henderson, Jackson, and Kerr (1982), and Colomb, Poppel, and Heiles (1980) were used to construct an all-sky map with 0°.5 resolution of the H I emission integrated in velocity, on the same grid as the infrared maps. Data from the Berkeley survey of the northern sky (Weaver and Williams 1973; Heiles and Habing 1974) were scaled by 1.15 to get the brightness temperature of the H I emission; enough overlap enabled us to scale the two other surveys to match the Berkeley observations. Since these surveys are significantly contaminated by "stray" radiation in the direction of weak H I emission (Lockman, Jahoda, and McCammon 1986), we used the lower resolution H I survey, made with the horn reflector of the Bell Laboratories (Stark *et al.* 1987), to discuss the correlation between infrared and H I emission in the polar caps (§ III*f*). Column densities of atomic hydrogen were derived from the H I data, assuming that the emission is optically thin.

c) CO Data

The comparison between infrared and CO emission (§ IV) is based on CO observations obtained with the northern and southern 1.2 m telescopes of the Goddard Institute for Space Studies and Columbia University; these observations have been put together in a single Galactic map by Dame *et al.* (1987).

d) Radio-Continuum Data

For the infrared–radio-continuum comparison (§ IV) we used the 408 MHz all-sky survey of Haslam *et al.* (1982). The resolution of this survey is comparable to the resolution of the *IRAS* all-sky maps. Following Phillipps *et al.* (1981) an extragalactic background of 6 K was subtracted from the data.

III. INFRARED EMISSION FROM ATOMIC AND DIFFUSE IONIZED GAS

The far-infrared emission of the Galaxy above $|b| > 10°$ is characterized by large-scale filamentary structures, resembling terrestrial cirrus clouds (Low *et al.* 1984), superposed on a continuous background (Hauser *et al.* 1984). From Galactic latitude profiles we demonstrate in § III*a* the existence of Galactic emission above 10° of latitude at 12 and 25 μm. We show in § III*b* that most of this emission in the mid-infrared comes from the interstellar medium. The correlation between far-infrared and H I emission is presented in § III*c*. We discuss the contribution of ionized gas and molecular clouds to the high-latitude emission in §§ III*d* and III*e*. The 100 μm observations are used in § III*f* to measure the extinction in the polar caps. The infrared luminosity coming from interstellar matter not associated with current star formation is derived in § III*g*.

a) Cosecant Laws

Galactic latitude profiles of the infrared and H I emission are presented in Figure 1. The profiles were built by averaging the pixels of the all-sky maps within 50 latitude bins with a width $\Delta(1/|\sin b|)$ of 0.1; data in the direction of the Magellanic Clouds, the main nearby molecular clouds and OB associations, and a few bright point sources were discarded when computing the profiles (see Table 1). At 60 and 100 μm the latitude profiles follow a cosecant law from 10° to the poles; the 12 and 25 μm brightness vary linearly with $1/|\sin b|$ from 10° to 30° and are constant above 30°. The absence of emission above 30° in the 12 and 25 μm profiles results directly from the

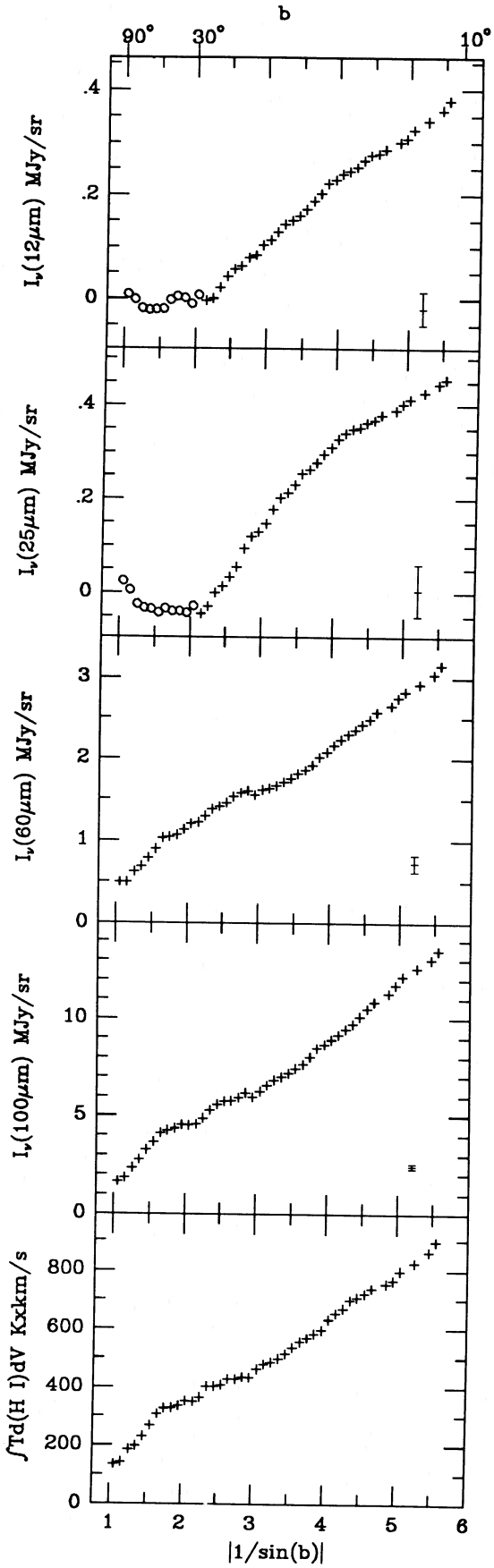

TABLE 1

REGIONS DISCARDED FOR COMPUTING THE GALACTIC LATITUDE PROFILES

Region	Limits in Galactic Coordinates
Carina	$245° < l < 275°$ $-20° < b < -10°$
Cepheus	$98° < l < 141°$ $10° < b < 22°$
Chamaeleon	$290° < l < 305°$ $-20° < b < -10°$
Large Magellanic Cloud	$273° < l < 286°$ $-38° < b < -30°$
Lupus-Ophiucus	$315° < l < 360°$ $10° < b < 30°$
Orion	$190° < l < 220°$ $-22.5 < b < -10°$
Perseus-Taurus	$150° < l < 170°$ $-32.5 < b < -10°$
Sagittarius	$0° < l < 50°$ $10° < b < 20°$
Small Magellanc Cloud	$300° < l < 307°$ $-47° < b < -43°$

assumption made in the subtraction of the zodiacal light, that the Galactic contribution to the 12 and 25 μm emission is negligible at high latitude (see Appendix A); consequently, the profiles of Figure 1 do not imply that there is no Galactic emission at 12 and 25 μm up to the Galactic poles.

The latitude profiles of Figure 1 prove the existence of Galactic emission outside the Galactic plane at all *IRAS* wavelengths. From the slopes of the cosecant laws, we derive the spectrum of the emission at $|b| > 10°$ presented in Figure 2 and listed in Table 2. The qualitative similarity between the energy distribution derived from the cosecant laws and the infrared spectra of nearby molecular and atomic clouds (Boulanger, Baud, and van Albada 1985, Weiland *et al.* 1986) suggests that the emission measured by the latitude profiles comes from the interstellar medium. This proposition is demonstrated in the following subsections.

b) Emission from Stars

The subtraction of the zodiacal light is not accurate enough to make a pixel-by-pixel correlation between the 12 and 25 μm emission and the distribution of interstellar dust, over the whole sky. However, one can indirectly prove that the 12 and 25 μm emission comes from the interstellar medium by showing that stars and circumstellar dust shells account for only a small fraction of the observed emission.

Counts of 12 μm point sources in different latitude strips, based on the *IRAS* catalog are presented in Table 3. From these counts we find that, at $|b| > 10°$, sources brighter than 0.7 Jy account for ~8% of the 12 μm flux measured by the

FIG. 1.—Profiles of infrared and H I emission for absolute latitudes larger than 10°. Data in the direction of the Magellanic Clouds and in the vicinity of the main nearby molecular clouds and OB associations and a few point sources were discarded when computing the infrared and H I profiles (see Table 1). A representative error bar on each individual infrared data point is plotted on the bottom-right corner of the infrared profiles. The uncertainties in the infrared profiles come mainly from the subtraction of the zodiacal light; the amplitude of these uncertainties was estimated by comparing the northern and southern half of the profiles after a rough subtraction of the Galactic emission associated with atomic gas.

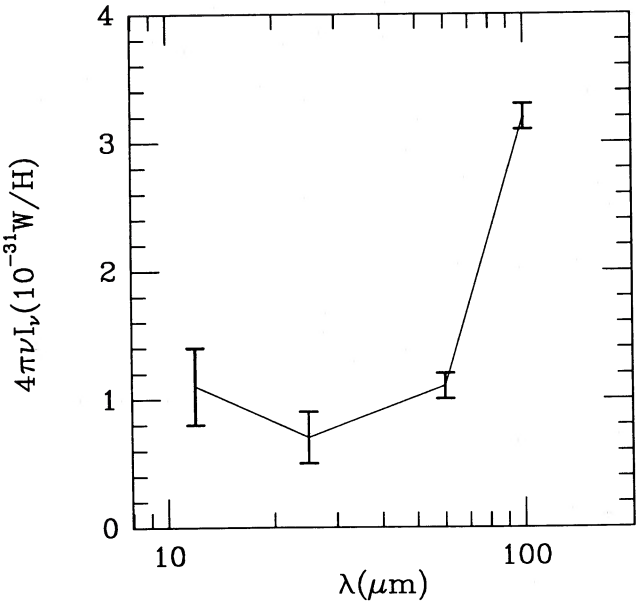

FIG. 2.—Infrared spectrum of emission at $|b| > 10°$ normalized per hydrogen atom. This spectrum is derived from the slopes of the cosecant laws presented in Fig. 1.

cosecant law; about one-third of this contribution comes from photospheres, two-thirds from stars with circumstellar dust shells. At 25 μm, point sources account for 2.5% of the observed brightness; this small contribution comes almost entirely from circumstellar dust shells. As essentially all stars at high latitude with circumstellar dust shells were detected by *IRAS* at 12 and 25 μm, counts in Table 3 are complete for dust shells. However, the counts need to be extrapolated to fainter sources to get the overall emission from photospheres. On the basis of a deep survey at $b = 30°$, Hacking and Houck (1987) found that the number of sources per decade of flux, $dN/d \log S$, from 10 to 500 mJy follows a power law with an index of 0.76 ± 0.11. Using this last index to extrapolate the counts of photospheres to fainter stars we find that point sources account for $10\% \pm 2\%$ of the 12 μm flux seen at $|b| > 10°$. This result depends only slightly on the index used to extrapolate the counts. Therefore, we can conclude that the 12 and 25 μm emission seen outside the Galactic plane comes almost entirely from the interstellar medium. A similar analysis led Ghosh, Drapatz, and Peppel (1986) to the same conclusion for the 12 and 25 μm emission from the Galactic plane.

TABLE 2

HIGH-GALACTIC-LATITUDE SPECTRUM

λ	Slopes[a]	$4\pi\nu I_\nu$[b] (10^{-31} W [H atoms]$^{-1}$)
12 μm	0.11 ± 0.03 MJy sr^{-1}	1.1 ± 0.3
25 μm	0.14 ± 0.04 MJy sr^{-1}	0.7 ± 0.2
60 μm	0.55 ± 0.03 MJy sr^{-1}	1.1 ± 0.06
100 μm	2.6 ± 0.1 MJy sr^{-1}	3.2 ± 0.12
H I	167 ± 5 K km s^{-1}	...
Total IR[c]	...	6.1 ± 0.7

[a] Slopes from the cosecant laws. For the infrared wavelengths the slopes refer to I_ν; for the H I, to the brightness temperature integrated in velocity. At 12 and 25 μm only the data at $|b| < 30°$ is used to measure the slopes.

[b] The normalization per hydrogen atom is done by dividing the slopes of the infrared cosecant laws by the slope of the H I cosecant law.

[c] Sum of $4\pi\nu I_\nu$ over the four *IRAS* wavelengths. This quantity is, for the spectrum of the inner Galaxy a good approximation of the infrared emission integrated from 5 μm to 1 mm (Paper II).

c) *Correlation between Far-Infrared and* H I *Emission*

Various examples of infrared cirri have been identified with local interstellar clouds (Low *et al.* 1984; Boulanger, Baud, and van Albada 1985; Terebey and Fich 1986; Weiland *et al.* 1986; de Vries, Heithausen and Thaddeus 1987) and regions of faint diffuse optical emission (de Vries and Le Poole 1985). These identifications suggest that the structure of the infrared emission is associated with interstellar clouds, heated by the interstellar radiation field of the Galaxy. We further investigate the origin of the infrared cirri by comparing, after subtraction of the large-scale Galactic latitude gradient, the 60 and 100 μm observations with the H I all-sky map. We computed for each pixel of the 60 μm, 100 μm, and H I maps the difference between the map value and the average brightness at the Galactic latitude of the pixel. A pixel-by-pixel comparison of these differences is presented in Figure 3; this figure shows a clear correlation between small-scale structures present in the

TABLE 3

12 μm POINT SOURCES AT HIGH GALACTIC LATITUDE

Galactic Latitude	Area[a] (sr)	N_{tot}[b]	N_1[b]	N_2[b]	N_3[b]	n[c]	$I_\nu(12\ \mu m)$[d] (Jy sr^{-1})	$I_\nu(25\ \mu m)$ (Jy sr^{-1})
$9\overset{\circ}{.}75 < \|b\| < 10\overset{\circ}{.}25$ ...	0.073	605	369	230	6	-0.97 ± 0.11	5.1×10^4	3.2×10^4
$14\overset{\circ}{.}5 < \|b\| < 15\overset{\circ}{.}5$	0.143	703	481	216	6	-0.95 ± 0.04	3.6×10^4	1.6×10^4
$27\overset{\circ}{.}5 < \|b\| < 32\overset{\circ}{.}5$	0.885	1933	1606	312	15	-0.93 ± 0.03	2.1×10^4	9.1×10^3
$\|b\| > 70°$	0.758	676	612	46	18	-0.92 ± 0.05	7.4×10^3	2.6×10^3

[a] Area over which sources were counted. In each latitude strip we discarded the same regions as for the computation of the cosecant laws in order to allow a direct comparison between the fluxes derived from these counts and the cosecant laws (see Table 1).

[b] The sources are sorted according to the following definitions: Photospheres—$S_\nu(12\ \mu m) > 2.5\ S_\nu(25\ \mu m)$, or $S_\nu(25\ \mu m)$ is an upper limit. Dust shells—Not a photosphere, and the source is detected at 60 and 100 μm, and $S_\nu(60\ \mu m) > S_\nu(100\ \mu m)$. Galaxies—Not a photosphere or a dust-shell. N_{tot} is the total number of sources brighter than 0.7 Jy; N_1, N_2, and N_3 are the number of photospheres, dust-shells, and galaxies, respectively.

[c] Index of a power-law fit to the number of sources per decade of flux; $dN/d \log S$ is fitted by S^n from 0.7 to 45 Jy. For these fits we did not separate photospheres from dust-shells.

[d] Brightness at 12 and 25 μm from point sources brighter than 0.7 Jy at 12 μm. These values were computed by dividing the total flux from the point sources by the area over which sources were counted; they must be compared to the cosecant laws (0.12 MJy sr^{-1})/sin($|b|$) and (0.14 MJy sr^{-1})/sin($|b|$) at 12 and 25 μm, respectively.

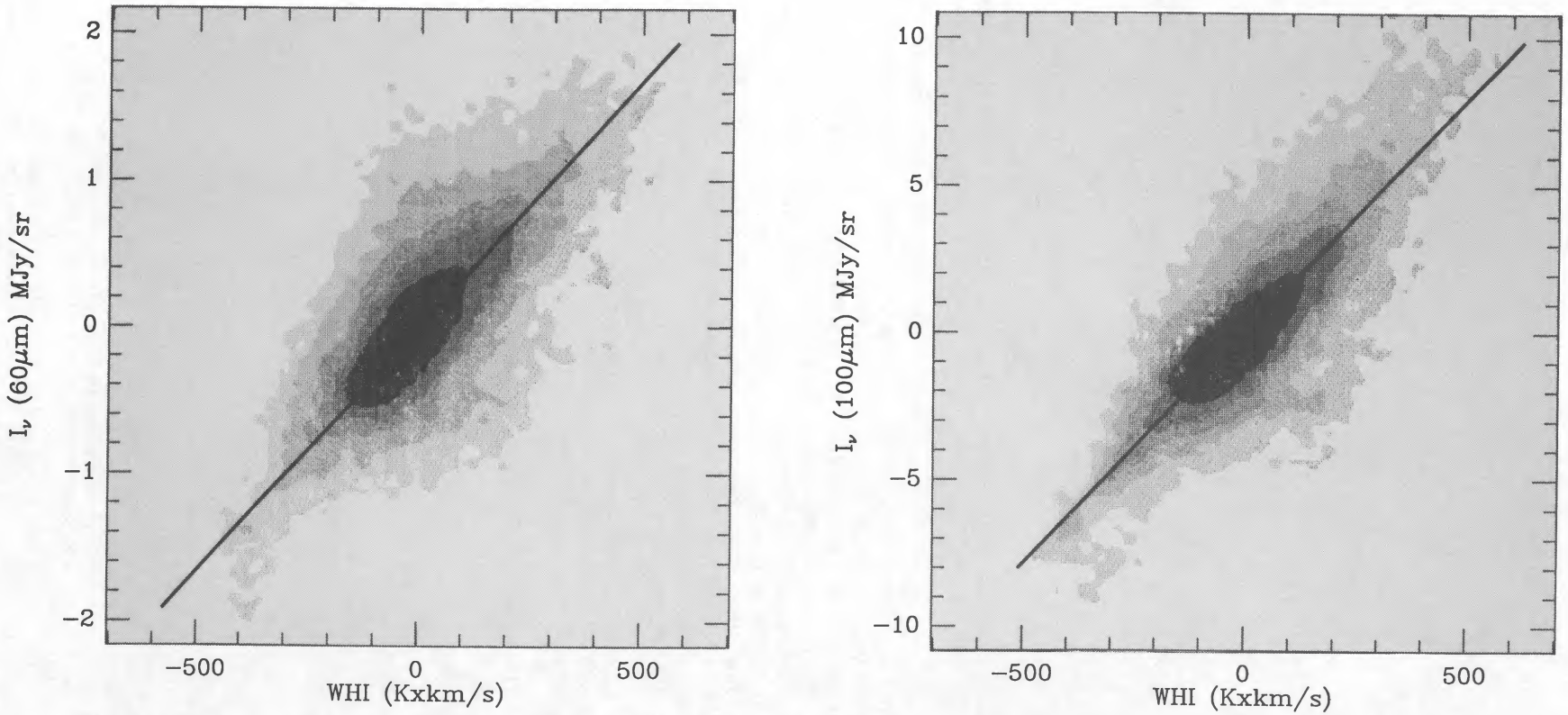

FIG. 3.—Correlation between infrared and H I outside the Galactic plane. For each pixel in the 60 μm, and H I all-sky maps, we computed the difference between the map value and the average emission at the Galactic latitude of the pixel. The two gray-scale plots show the density distribution of these differences in a 60 μm–H I and a 100 μm–H I diagram. The straight lines superposed on the gray-scale plots go through the origin and have a slope equal to the ratio of 60 and 100 μm to H I emission derived from the cosecant laws (Table 2). Pixels below 10° of Galactic latitude, in the Magellanic Clouds, and in the vicinity of the main molecular clouds and OB associations listed in Table 1 were discarded.

infrared and H I maps which proves that most infrared cirri have a counterpart in the distribution of the H I emission.

The straight lines on the 60 μm H I and 100 μm H I diagrams represent the infrared emissivity per H atom derived from the cosecant laws; the fact that these lines approximately follow the major axis of the distribution of points implies that the smooth background arises mainly from dust associated with neutral atomic gas. The scatter of the points around the lines derived from the cosecant laws is ~ 2 times larger than what is expected from the uncertainties on the infrared and H I data. Part of the observed dispersion results from the presence of molecular clouds at high Galactic latitude (§ III*e*), and possibly from structures in the distribution of the ionized gas (§ III*d*). A significant fraction of the scatter is also due to the fact that the infrared emission per H atom varies from place to place in the solar neighborhood.

We investigated the variations of the ratio between infrared and H I emission by comparing 60 and 100 μm observations with H I data over limited regions of the sky. In this comparison, lines of sight crossing molecular clouds were avoided on the basis of the CO observations presented by Dame *et al.* (1987). Figure 4 illustrates the correlation between the far-infrared and H I emission in Orion, Figure 5 the correlation between 100 μm and H I emission at $|b| > 50°$. Similar comparisons were also made in the Auriga and Lupus constellations chosen as examples of low and high ratios between infrared and H I emission. The results of linear least-square fits between the infrared and H I data are listed in Table 4. The good correlation observed within each field proves that, on scales of the order of 100 pc, the interstellar radiation field and the dust abundance are reasonably uniform. On the other hand, we find variations of the far-infrared emission per H atom by a factor of 3 from one field to the other. The fact that the highest values of the emissivity are observed in the vicinity of OB associations, while low values are seen in the direction of the anticenter suggests that changes in the infrared emission per H atom are mainly due to variations in the intensity of the interstellar radiation field. The 60/100 μm color ratio is close to the average value of 0.21 obtained from the slopes of the cosecant laws for all fields except the polar caps where we measured a higher ratio. Since in the polar caps the $I_\nu(100\ \mu\text{m})/N_H$ ratio is similar to the value derived from the cosecant laws we do not see any clear explanation for this color difference. For the other fields, assuming that variations in the $I_\nu(100\ \mu\text{m})/N_H$ ratio trace primarily changes in the intensity of the radiation field, the constancy of the 60/100 μm color suggests that small grains heated transiently by individual photons account for a significant fraction of the 60 μm emission (see § VIII).

d) Emission from Diffuse Ionized Gas

Observations of Hα emission at high Galactic latitude (Sivan 1974; Reynolds 1984) and dispersion measurements in the direction of pulsars (see, e.g., Harding and Harding 1982) indicate that a significant fraction of the gas outside discrete H II regions is ionized; dispersion measures imply that the local surface density of ionized hydrogen outside H II regions is of the order of 1.2 $M_\odot$ pc^{-2}, which represents 20% of the total density of neutral plus ionized hydrogen; this value is a lower limit if the scale height of the ionized gas is more than ~ 1 kpc because there are essentially no pulsars to probe the distribution of electrons above this height (Kulkarni and Heiles 1986). Therefore, unless there is a difference in dust abundance between ionized and neutral gas, dust associated with the diffuse ionized gas accounts for $\sim 20\%$ of the infrared emission measured by the cosecant laws; for an emissivity similar to that for the neutral gas we expect the emission from the ionized gas to be 0.6 MJy sr^{-1} in average over the polar caps. The ratio between 100 μm and H I emission at $b > 50°$ and $b < -50°$ was derived in § III*c* from the correlations shown in Figure 5 (Table 4). If we scale the latitude distribution of H I emission by this number we get a latitude profile which differs from the profile of infrared emission by much less than the 20% contribution expected from diffuse ionized gas (Fig. 6). As the H I and 100 μm profiles agree closely at all latitudes, this problem cannot be solved by simply changing the zero level of the Galactic emission (§ II). We see two possible explanations to this result: (1) the diffuse ionized gas is deficient in dust; (2) the distribution of the ionized gas is correlated with the distribution of the H I gas. In this last case the infrared emissivities derived from the correlation in Figure 5 include the contribution of the ionized gas. Note about this point that at $|b| > 50°$ there is hardly any large-scale variation of the emission with the Galactic latitude and that the correlation observed in Figure 5 is a correlation between localized structures in the infrared and H I maps.

TABLE 4

INFRARED–H I CORRELATION

Region	Limits in Galactic Coordinates	$I_\nu(60\ \mu\text{m})/N_H$[a]	$I_\nu(100\ \mu\text{m})/N_H$[a]	$I_\nu(60\ \mu\text{m})/I_\nu(100\ \mu\text{m})$[b]
Cosecant Laws	$\lvert b\rvert > 10°$	0.18 ± 0.01	0.85 ± 0.05	0.21 ± 0.02
Auriga	$150° < l < 170°$, $15° < b < 30°$	0.107 ± 0.014	0.51 ± 0.05	0.21 ± 0.02
Lupus	$330° < l < 345°$, $10° < b < 20°$	0.55 ± 0.10	2.4 ± 0.5	0.23 ± 0.01
Orion	$200° < l < 230°$, $-30° < b < -20°$	0.27 ± 0.04	1.3 ± 0.1	0.21 ± 0.01
$b = 30°$	$27°.5 < b < 32°.5$	0.26 ± 0.08	1.4 ± 0.2	0.19 ± 0.03
$b = -30°$	$-32°.5 < b < -27°.5$	0.20 ± 0.05	1.1 ± 0.1	0.18 ± 0.03
Northern galactic cap	$b > 50°$	0.26 ± 0.06	0.92 ± 0.14	0.29 ± 0.05
Southern galactic cap	$b < -50°$	0.24 ± 0.07	0.79 ± 0.06	0.30 ± 0.08

[a] The infrared emission to H I column density ratios are in units of MJy sr^{-1} (10^{20} H atoms)$^{-1}$ cm^2. In each case two linear regressions were done using the infrared and H I data as the independent variable, respectively; the error bar covers the two values derived from these fits. Values obtained from the slopes of the cosecant laws (Table 2) are listed for comparison.

[b] These colors are derived from a direct correlation between the 60 and 100 μm fluxes, and not from the results of the infrared–H I correlation.

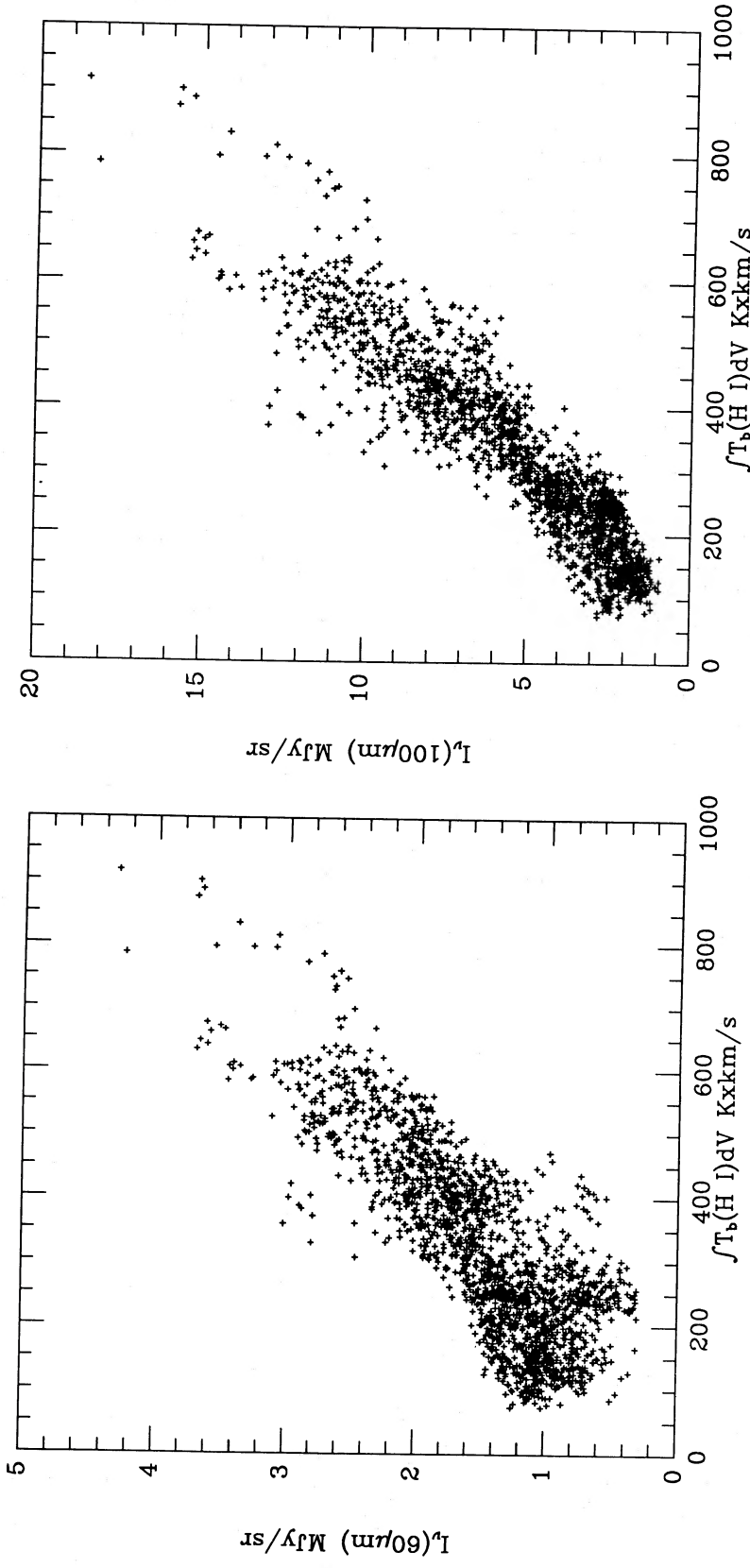

FIG. 4.—Pixel-by-pixel comparison between far-infrared (60 and 100 μm) and H I emission over a field of a few hundred square degrees in Orion. Each cross represents a 0°.5 × 0°.5 pixel.

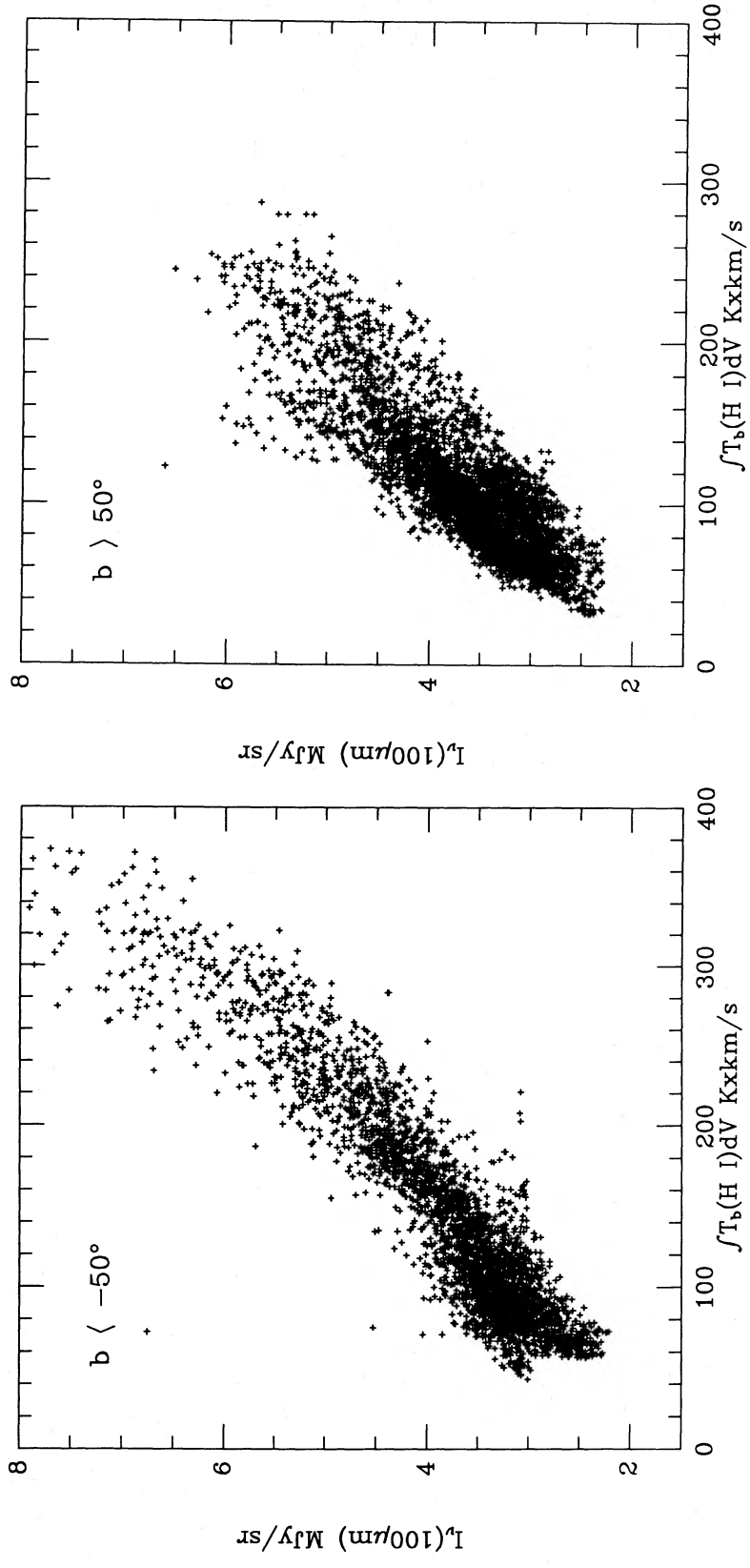

FIG. 5.—Pixel-by-pixel comparison between 100 μm and H I emission around the north and south Galactic pole. To avoid contamination by stray radiation, we used for this comparison the H I survey made with the horn reflector of the Bell Laboratories. The 100 μm data were smoothed to the lower resolution of this survey; each pixel represents a 1°.5 × 1°.5 pixel.

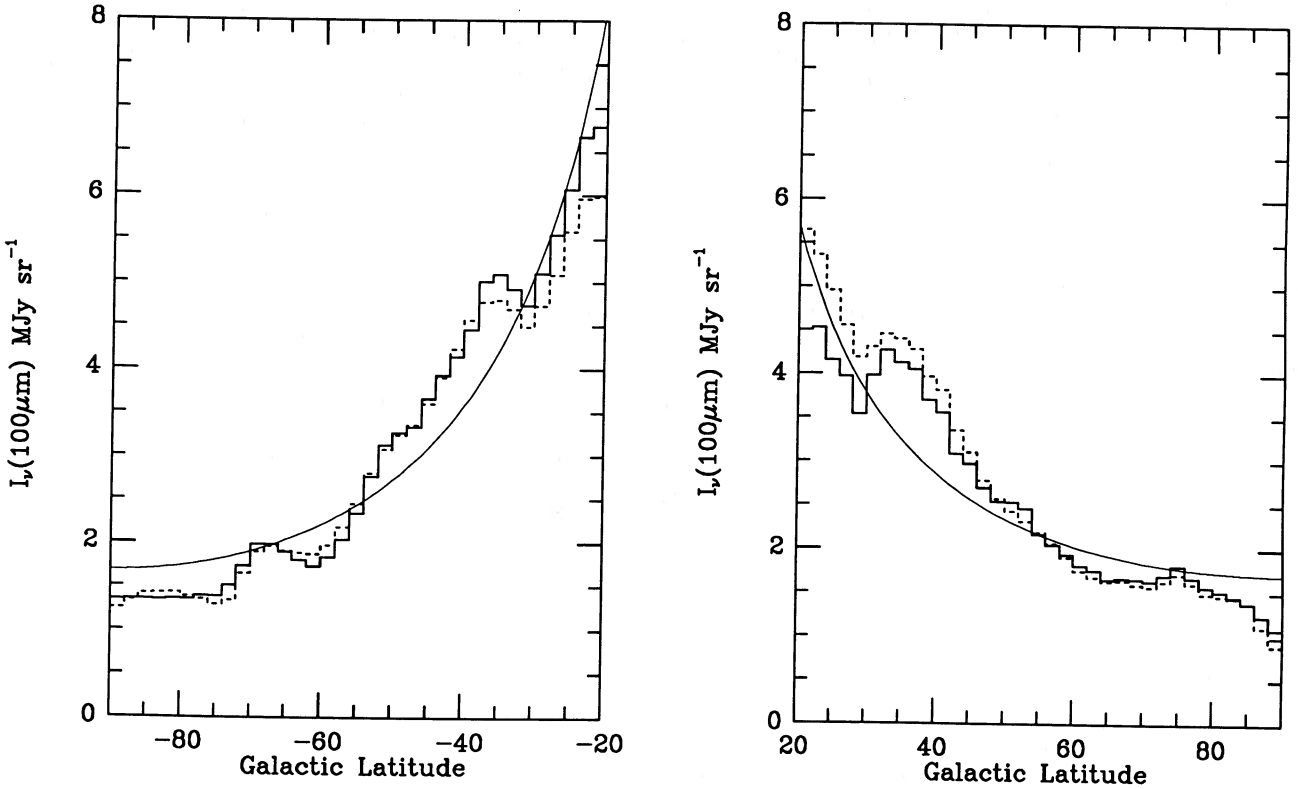

FIG. 6.—Galactic latitude profile of the 100 μm emission at $b < -20°$ and $b < -20°$. In each plot, the histogram drawn with a solid line represents the profile of the 100 μm emission; the dotted line represents the profile of the integrated H I emission derived from the survey of the Bell Laboratories; the H I profiles are scaled by the 100 μm/H I ratios derived from the 100 μm–H I correlation at $b > 50°$ and $b < -50°$ (Table 4). In each plot the continuous line represents a least-squares fit of the 100 μm profile by a cosecant law (see text). The southern profiles, 100 μm and H I, were computed by averaging data only over the part of the sky which is covered by the H I survey of the Bell Laboratories.

e) Emission from High-Latitude Molecular Clouds

Weiland *et al.* (1986) and de Vries, Heithausen, and Thaddeus (1987) have identified several infrared cirri with high–Galactic latitude molecular clouds and measured a ratio between 100 μm and CO emission of 1.0 ± 0.5 MJy sr^{-1} (K km s^{-1})$^{-1}$. This ratio can be put together with the CO survey of Magnani, Blitz, and Mundy (1985) to estimate the contribution of dust associated with high–Galactic latitude molecular clouds to the infrared emission of the local interstellar medium. Magnani, Blitz, and Mundy estimated the total CO emission at $|b| > 20°$ to be $0.10/e$ (K km s^{-1}) sr, where e is the fractional completeness of the survey. Assuming $e = 0.5$, we find that the total 100 μm emission at $|b| > 20°$ coming from high–Galactic latitude clouds is of the order of 0.2 MJy, which represents 0.6% of the total 100 μm emission observed over the same range of latitudes. This small fraction simply results from the fact that the small molecular clouds seen at high Galactic latitude represent a negligible fraction of the interstellar gas in the solar neighborhood: the surface density is of the order of 0.1 $M_\odot$/pc^2 while the surface density of H I gas is $\sim 5\ M_\odot$ pc^2.

f) Infrared Emission in the Polar Caps

Gray-scale maps of the 100 μm emission around the northern and southern Galactic poles are presented in Figure 7. The latitude profiles of Figure 6 and the scatter diagrams of Figure 5 show that there is a good correlation between the distribution of the 100 μm and H I emission in the polar caps ($|b| > 50°$). The average $I_\nu(100\ \mu m)/N_H$ ratio of 0.85 MJy sr^{-1} for 10^{20} H atoms cm^{-2} is equivalent to a $I_\nu(100\ \mu m)/A_v$ ratio of 15.9 MJy sr^{-1} mag^{-1} for the standard A_v/N_H ratio of 5.3×10^{-22} mag cm^2 (Bohlin, Savage, and Drake 1978). These numbers can be used to convert the 100 μm brightness to gas column densities or visual extinctions. For these numbers, the sensitivity limit of *IRAS* at 100 μm corresponds to the emission associated with a column density of gas of a few 10^{19} H atoms cm^{-2} or an A_v of 0.01 mag.; however, the uncertainties on absolute measurements are larger due to uncertainties in the subtraction of the zodical light, estimated to $\sim$0.5 MJy sr^{-1} (see Appendix A), which corresponds to $A_v \approx 0.03$ mag, and due to uncertainties in the zero level of the Galactic emission if there is any ionized gas in the holes of H I emission (see § III*d*); we estimate this last uncertainty to 0.6 MJy sr^{-1} (§ II).

To study the distribution of the extinction in the polar caps we made a histogram of the 100 μm emission at $|b| > 50°$ (Fig. 8). The histogram peaks at 1.6 MJy sr^{-1}, 20% of the points are below 1.3 MJy sr^{-1} and 80% below 2.4 MJy sr^{-1}; the median value is 1.7 MJy sr^{-1}. Converting these numbers to visible extinctions, we get a median extinction $A_v = 0.11^{+0.06}_{-0.03}$ mag; 20% of the polar caps have $A_v < 0.08^{+0.06}_{-0.03}$ mag, and 80% have $A_v < 0.15^{+0.06}_{-0.03}$; regions of low extinction can be readily identified on the maps of Figure 7. The visible extinction is $0.05^{+0.06}_{-0.03}$ and $0.07^{+0.06}_{-0.03}$ at the northern and southern Galactic poles, respectively. The uncertainties in these measurements are too large to completely settle the existing debate over the existence of windows free of obscuration in the polar caps (Sandage 1973; de Vaucouleurs and Buta 1983). De Vaucouleurs and Buta derived their estimate of the extinction at the pole from the slope of a cosecant fit to the latitude distribution of the

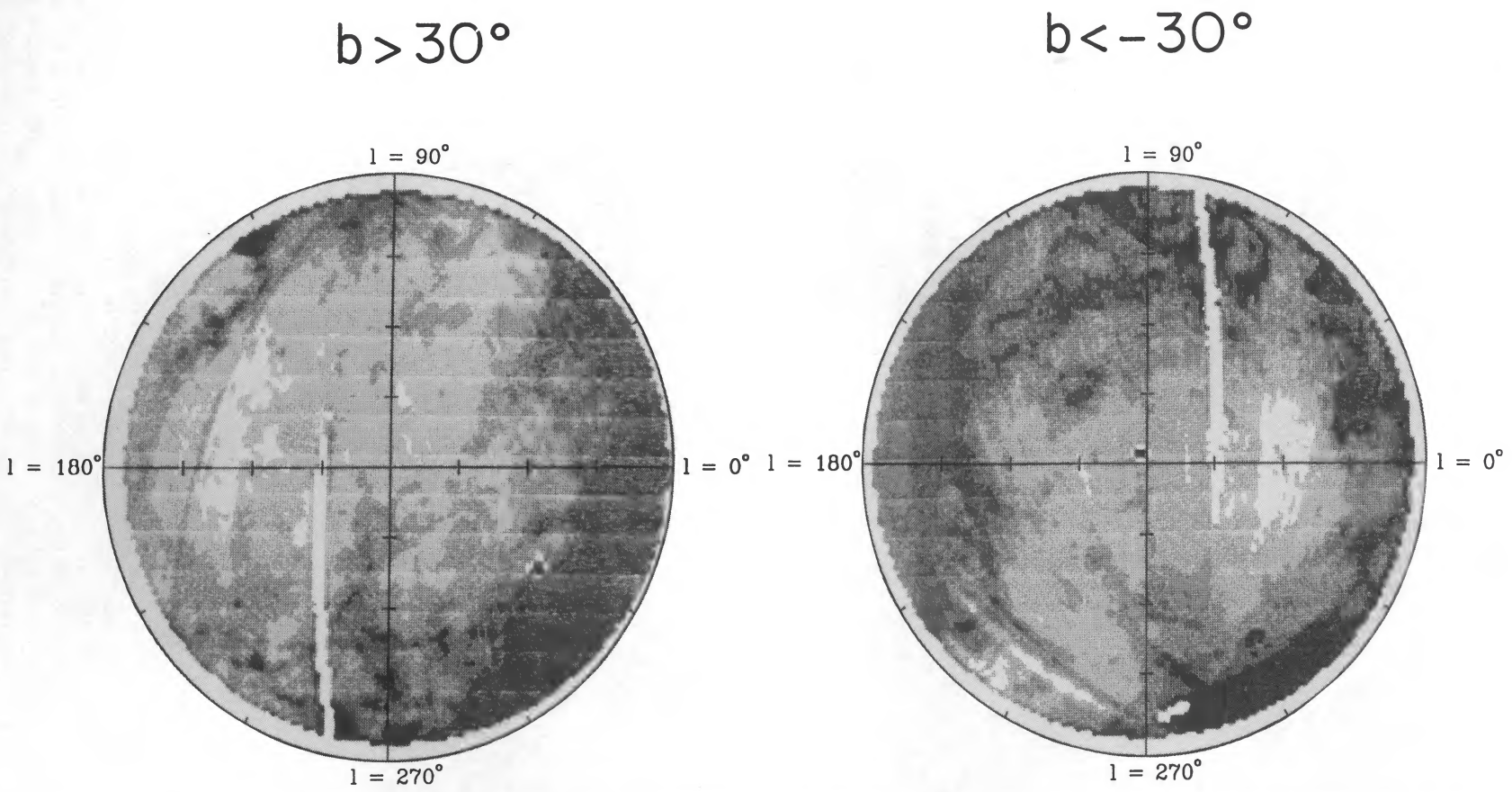

FIG. 7.—Gray-scale maps of the 100 μm emission around the northern and southern Galactic poles ($|b| > 30°$); tick marks on the axis are spaced by 15°. The bright source near south Galactic pole is the spiral galaxy NGC 253. The resolution of the maps is 1°.5. The gray-scale maps are white for $A_v < 0.06$ mag.; the three levels of gray correspond to the range of A_v: $0.06 < A_v < 0.14$ mag, $0.14 < A_v < 0.20$, and $0.20 < A_v < 0.30$ mag; regions in black have an $A_v > 0.30$ mag; positive error bar on these measurements is 0.06 mag; the negative error bar is 0.03 mag.

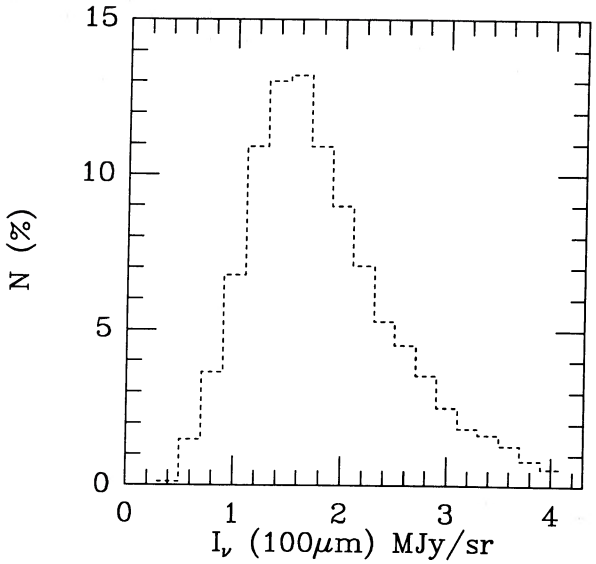

FIG. 8.—Histogram of Galactic emission at $|b| > 50°$

extinction at $|b| > 20°$. The validity of this procedure may be tested with the *IRAS* data. Linear least-square fits to the 100 μm latitude profiles at $b > 20°$ and $b < -20°$ (Fig. 6) give the following cosecant laws:

$$I_\nu(100\ \mu\text{m}) = (3.4 \pm 0.2)/|\sin(b)| - 1.7 \pm 0.25\ \text{MJy sr}^{-1} \text{ for } b < -20°,$$

$$I_\nu(100\ \mu\text{m}) = (2.1 \pm 0.2)/|\sin(b)| - 0.4 \pm 0.2\ \text{MJy sr}^{-1} \text{ for } b > 20°,$$

while the 100 μm emission at the northern and southern Galactic poles is 1.1 ± 0.5 MJy sr^{-1} and 1.3 ± 0.5 MJy sr^{-1} if there is no 100 μm emission from ionized gas in the holes of H I (§ II). Within this assumption we find that the polar brightnesses are significantly smaller than the slopes of the cosecant laws. However we could be underestimating the 100 μm emission at the poles by ~ 0.6 MJy sr^{-1} if the 100 μm emissivity of the ionized gas is similar to that of the H I gas, and if the holes of H I emission are not also holes in the distribution of ionized gas (see § III*d*).

g) Contribution to the Infrared Luminosity of the Solar Neighborhood

In Table 2 we estimated the bolometric emission of dust by summing νI_ν at the four wavelengths (Paper II) and derived an emission per hydrogen atom of 6.1×10^{-31} W(H atom)$^{-1}$; $\sim 60\%$ of this radiation is radiated between 8 and 120 μm, i.e., within the range of wavelengths covered by *IRAS*. The infrared emission per hydrogen atom corresponds to an infrared-luminosity–to–mass-of-neutral-atomic-gas ratio, L_{IR}/M_H, of 1.9 $L_\odot/M_\odot$; if the diffuse ionized gas at high latitude has an infrared emissivity similar to that for neutral atomic gas (§ III*d*) the infrared emission per nucleon is 4.9×10^{-31} W(H atom)$^{-1}$ equivalent to an L_{IR}/M_H ratio of 1.5 $L_\odot/M_\odot$. This ratio measures the average emissivity of the interstellar medium away from OB associations, within a distance of ~ 500 pc from the Sun. By scaling this emissivity by the local surface density of H I and H II gas, 6 $M_\odot$ pc^{-2}, we get an infrared luminosity per unit surface of 9 $L_\odot$ pc^{-2}. This luminosity is compared with the contribution of H II regions and molecular clouds in § VI.

The amount of stellar light absorbed by interstellar dust may be calculated from the interstellar radiation field (ISRF) spectrum, the extinction curve, and albedo measurements; using numbers tabulated by Mathis, Mezger, and Panagia (1983), we find that interstellar dust absorbs $\sim 4.6 \times 10^{-31}$ W(H atoms)$^{-1}$ a number which is in close agreement with the total infrared emission per nucleon derived from the *IRAS* data.

IV. INFRARED EMISSION FROM MOLECULAR CLOUDS

Dust in molecular clouds is heated both by embedded stars and the interstellar radiation field of the Galaxy (ISRF). We discuss in § IV*a* the heating of molecular clouds by the external radiation and show that it places a lower limit on the ratio between infrared luminosity and mass of gas which depends only on the optical depth of the cloud. In § IV*b* we show that, for the average star-formation efficiency of the solar neighborhood, the overall luminosity of nonionizing embedded stars is negligible with respect to the luminosity absorbed from the ISRF. On the other hand, for clouds forming high-mass stars the luminosity of only one ionizing star ($M^* > 20\ M_\odot$) is comparable to the luminosity a giant molecular cloud (GMC) absorbs from the external radiation field. Infrared and CO emission of molecular clouds are compared in § IV*c*. The overall luminosity of molecular clouds in the solar neighborhood is estimated in § IV*d*.

a) Heating by the ISRF

As molecular clouds are partly optically thick to the external radiation, the contribution of the ISRF to the infrared emission depends on the geometry and optical depth of the clouds. Flannery, Roberge, and Rybicki (1980) addressed numerically the radiative transfer equations in the simple case of a uniform, spherical cloud heated from outside by a uniform radiation field. Mathis, Mezger, and Panagia (1983) made use of an analytical fit to the numerical solution to study the variation of the heating rate per grain across clouds of different optical depths. We repeated their calculations for spherical clouds of total $A_v = 2$, 5, and 10 and computed the average heating rate along the line of sight as a function of the impact parameter. By multiplying the average heating rate by the column density of dust we get the total energy absorbed by dust grains along the line of sight, a quantity equal to the total emission of dust integrated over infrared and submillimetric wavelengths. Grain properties—extinction and albedo—and the ISRF spectrum were taken from Mathis, Mezger and Panagia (1983). In a first set of calculations we assumed that the radiation field at the surface of the cloud is equal to the average ISRF. In a second set we assumed that the radiation field is attenuated by an envelope of $A_v = 0.5$ mag which is supposed to protect the molecules from photodissociation by ultraviolet photons; in this case the ultraviolet light at the surface of the cloud is attenuated by a factor 6 compared to the ISRF; this attenuation is due to the envelope and the shadowing effect of the cloud over half the sky. The results of both models are presented in Figure 9*a*; for each model separate lines corresponding to different clouds approximately line up to produce a relation between total infrared emission and extinction roughly independent of the total optical depth of the cloud. In the limit of an optically thin cloud, the calculations give a total infrared emission of 4.6×10^{-31} W per nucleon, or 8.7×10^{-6} W m^{-2}

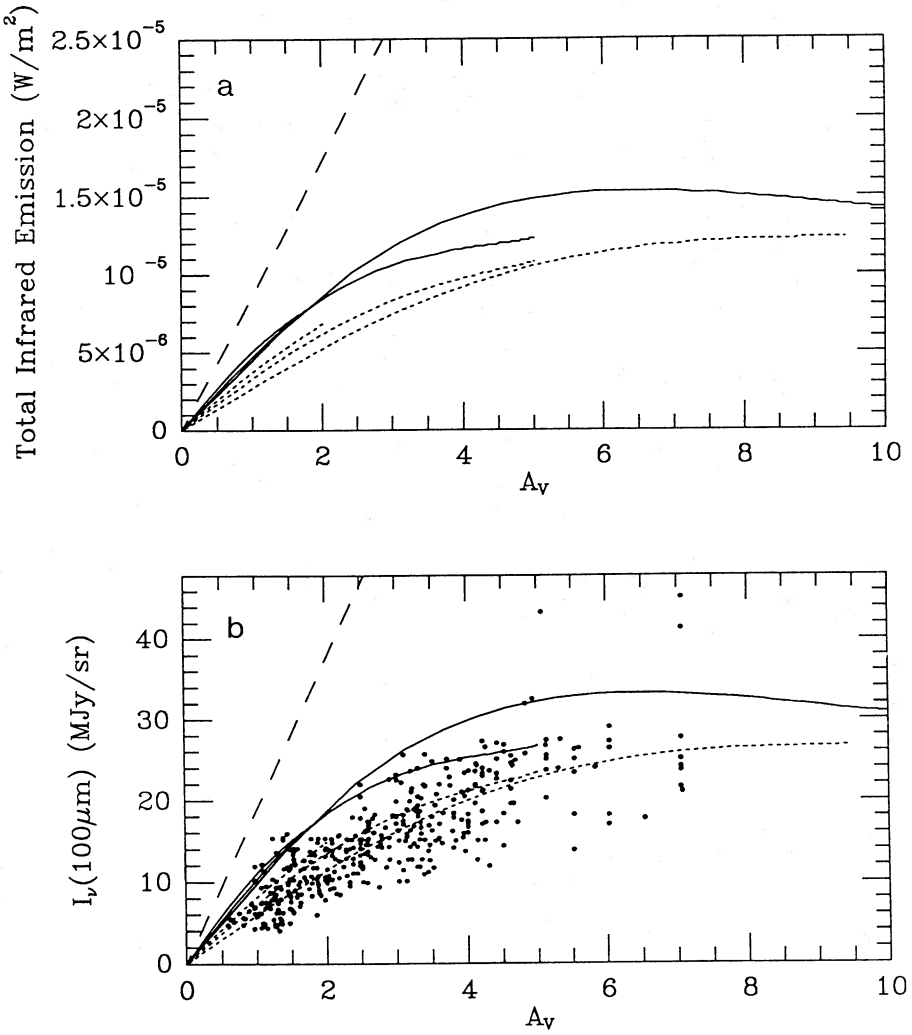

FIG. 9.—Infrared emission versus visible extinction. (*a*) The results of a model of the infrared emission from a uniform, spherical cloud heated from outside by a uniform radiation field. Results are shown for clouds of total optical depth through the center: $A_v = 2$, 5, and 10. Two sets of curves are presented; solid lines give the results of the model in the case where the heating radiation field is the average ISRF; for the dotted lines the radiation field at the surface of the cloud is attenuated by an envelope of $A_v = 0.5$ mag. The dashed line gives the slope of the linear relation between total infrared emission and A_v in the case of an optically thin cloud. In (*b*) the results of the model are compared with 100 μm and A_v data for the Heiles 2 cloud in Taurus, taken from Cernicharo and Guélin (1987).

per magnitude of visual extinction; these numbers are in good agreement with the observed values derived from the cosecant laws (§ III*g*).

Data for the Heiles 2 cloud in Taurus taken from Cernicharo and Guélin (1987) are compared with the model in Figure 9*b*, where the curves of figure 9*a* have been scaled in order to get a 100 μm brightness of 18.7 MJy sr^{-1} per magnitude of visual extinction in the optically thin case; this emissivity is derived from a correlation of IR and H I data in the Taurus region (Boulanger *et al.* 1988*b*). Other dark clouds for which similar data are available (de Vries and Le Poole 1985; Boulanger *et al.* 1988*b*) follow the same general relation. An important feature of the curves and the data presented in Figure 9*b* is the approximate linearity of the relation between 100 μm emission and extinction for $A_v < 3$ mag. This linearity implies that the 100 μm emission is a good tracer of the column density of dust over regions of moderate extinction; assuming a uniform dust-to-gas ratio, the 100 μm *IRAS* data can thus be used to map the distribution of molecular gas in the solar neighborhood outside star-forming regions and dense condensations. The comparison between 100 μm and A_v data in Taurus indicates that the 100 μm emission of the molecular cloud is ~ 5 MJy sr^{-1} per magnitude of visible extinction which is a factor 4 smaller than what is measured for the atomic gas in the same region. This difference indicates that the radiation field is significantly attenuated inside the molecular cloud. The comparison between model and data in Figure 9*b* suggests that shielding by the molecular cloud dust is not sufficient to produce the right attenuation; a good agreement is reached only when we take into account an additional attenuation by an envelope of $A_v = 0.5$ mag.

Values of the infrared-luminosity–to–mass-of-molecular-hydrogen ratio, L_{IR}/M_{H_2}, may be derived from the model; without the envelope we find that L_{IR}/M_{H_2} is equal to 54%, 36%, and 25% of the optically thin value, for clouds of total visible extinction 2, 5, and 10, respectively; with the 0.5 mag envelope, the same ratios are 37%, 25%, and 18%. Using the average L_{IR}/M_H of the local H I gas, 1.5 $L_\odot/M_\odot$, as the optically thin value, we get ratios of infrared luminosities to mass of gas in the range 0.3–0.8 $L_\odot/M_\odot$.

The comparison between model and data made in Figure 9*b* assumes that the spectrum of the infrared emission does not change from the center to the surface of the clouds. However, the external radiation gets attenuated as it penetrates the cloud, and grains deep inside a cloud are colder than grains in optically thin parts of the interstellar medium. The importance of this effect depends critically on the equilibrium temperature of grains heated by the ISRF because the ratio between the emission in the 100 μm band of *IRAS* and the bolometric infrared emission drops dramatically with temperature below 18 K for an emissivity proportional to ν^2 and below 21 K for an emissivity proportional to ν (Boulanger *et al.* 1988*b*); to provide an example, for an emissivity proportional to ν^2 the ratio between 100 μm in-band flux and total infrared emission is 0.28 ± 0.04 for $18\ \mathrm{K} < T < 32\ \mathrm{K}$, but only 0.15 at 15 K and 0.06 at 12 K. Since part of the 60 μm emission is probably coming from small grains (§ VIII) the 60/100 μm color cannot be used to estimate the equilibrium temperature of big grains and to assess the importance of this effect, but qualitatively one has to keep in mind that $I_\nu(100\ \mu\mathrm{m})$ may saturate faster with increasing A_v than indicated by Figure 9*b*. In the comparison between model and data this effect may be compensated for by the fact that the model does not take into account the inhomogeneity of molecular clouds, which allows the external radiation to penetrate deeper into the cloud (Natta and Panagia 1984).

b) Heating by Embedded Stars

To understand the origin of the infrared emission from molecular clouds the luminosity absorbed from the ISRF must be compared to the luminosity from embedded stars. The star-formation rate and initial mass function (IMF) in the solar neighborhood has been estimated from star counts by various authors (Miller and Scalo 1978; Lequeux 1979; Garmany, Conti, and Chiosi 1982; Scalo 1986); their results can be approximated by the following analytical expressions:

$$\frac{d^2N}{d\ln M\, dt} = 1. \times 10^{-9}\, M^{-1.7} \text{ stars yr}^{-1}\, M_\odot{}^{-1} \quad \text{for } 2\ M_\odot < M < M_{up}$$

$$= 0.5 \times 10^{-9}\, M^{-0.7} \text{ stars yr}^{-1}\, M_\odot{}^{-1} \quad \text{for } M < 2\ M_\odot\ ,$$

where the star-formation rate has been normalized per unit mass of molecular hydrogen, using a local surface density of molecular hydrogen of 1.3 $M_\odot$ pc^{-2} (Dame *et al.* 1987). For this IMF and different durations of constant star formation, we show in Figure 10 how the luminosity and total mass of main-sequence stars depend on the upper cut-off of the IMF, M_{up}. After 10^7 yr, it is only for values of M_{up} larger than 10 $M_\odot$ (mass of a B2 star) that the luminosity of embedded stars goes over the L_{IR}/M_H threshold of $\sim 0.5\ L_\odot/M_\odot$ set by the ISRF heating. This result, which depends only weakly on the actual time stars stay associated with the parent cloud, shows that on average low-mass stars have a negligible contribution to the infrared luminosity of molecular clouds.

Integrating the IMF from M_* to infinity, we get the following expression for the number of stars of mass larger than M_* formed by a cloud of mass M_{H_2} over 10^7 yr:

$$N(M > M_*) = 3.6(M_*/20\ M_\odot)^{-1.7}(M_{H_2}/10^5\ M_\odot) \quad \text{for } M_* > 2\ M_\odot\ .$$

Only giant molecular clouds with masses larger than 10^5 $M_\odot$ have a high probability of forming a high-mass star which will develop an H II region. The luminosity of only one of these high-mass stars, $\sim 5.2 \times 10^4 (M_*/20\ M_\odot)^2$, is comparable to the luminosity a GMC absorbs from the ISRF. Therefore, the

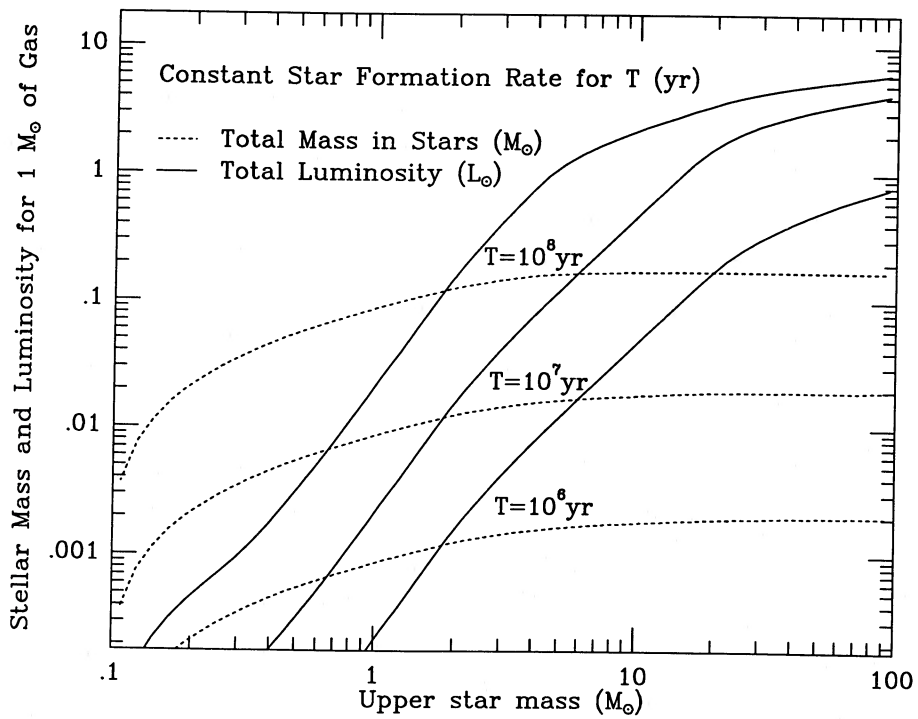

FIG. 10.—Luminosity and total mass of main-sequence stars vs. upper cutoff of the IMF. These curves were computed for the IMF, normalized per unit mass of molecular hydrogen, given in the text. The different curves correspond to different durations of constant star formation.

infrared emission of GMCs associated with H II regions comes from the most massive stars formed by the cloud. Studies of infrared sources in the Galactic plane (Caux *et al.* 1985; Myers *et al.* 1986; Solomon *et al.* 1987) show that GMC–H II region associations are the most luminous infrared sources in the Galaxy. These associations have infrared-luminosity–to–mass-of-gas ratios larger than 1 $L_\odot/M_\odot$, up to several tens of $L_\odot/M_\odot$.

c) *Comparison of Infrared and* CO *Observations*

The above discussion suggests that the infrared emission of molecular clouds can be written as the sum of two terms: the first, correlated with the column density of gas, represents the heating of dust by the ISRF; the second, associated with embedded stars, is significant only close to regions of star formation and on average is negligible for clouds that do not contain any high-mass stars. Maps of the 100 μm emission of the main nearby molecular clouds have been presented and compared with large scale CO, ^{13}CO, A_v data by Boulanger *et al.* (1988*b*). A good correspondence is observed between the CO and infrared pictures of the clouds; outside regions of star formation and dense condensations the 100 μm emission is well correlated with A_v measurements and the integrated CO emission. The 100 μm–CO diagrams of Orion A and Chamaeleon II chosen as examples of clouds of high and low star-formation activity (Fig. 11), illustrate the results of this comparison. For clouds like Chamaeleon II that are largely devoid of star formation, the infrared emission is dominated by the external heating and correlates with the CO emission.

In more active clouds, like Orion A, the comparison of infrared and CO emission leads to a more intricate pattern. At the bottom of the 100 μm–CO diagram, points outside star-forming regions define a lower envelope which shows that infrared and CO emission are correlated in these directions. Points representing lines of sight in the direction of star-forming regions appear scattered above the lower envelope; the radiation absorbed from embedded or very nearby stars is for these points comparable to, or much greater than, the emission associated with the external heating; many of these points do not appear on the diagram of Figure 11 because the 100 μm brightness is larger than 45 MJy sr^{-1}. Pixels within 20 MJy sr^{-1} from the lower envelope account for 77% of the surface of the cloud and 64% of the CO emission but only 12% of the IR luminosity; the overall infrared-luminosity–to–mass-of-molecular-hydrogen ratio, L_{IR}/M_{H_2}, is 2.1 $L_\odot/M_\odot$ for the lines of sight corresponding to these pixels and 16 $L_\odot/M_\odot$ for the other lines of sight. The lower envelope of the Orion diagram extends to higher values of integrated CO emission (W_{CO}) than the correlation seen in the Chamaeleon II diagram. The high values of integrated CO emission probably correspond to regions of higher excitation in the vicinity of embedded stars. Therefore, the high-W_{CO} part of the lower envelope should not be interpreted as a simple extension to high A_v of the correlation between infrared emission and column density of gas.

Most molecular clouds show 12, 25, and 60 μm emission over an extent similar to the 100 μm emission. However, the color ratios vary from cloud to cloud in a manner which is not obviously related to the star-formation activity of the clouds (see Table 5).

d) *Contribution to the Infrared Luminosity of the Solar Neighborhood*

An extensive comparison of CO and *IRAS* observations of nearby molecular clouds has been carried out by Boulanger *et*

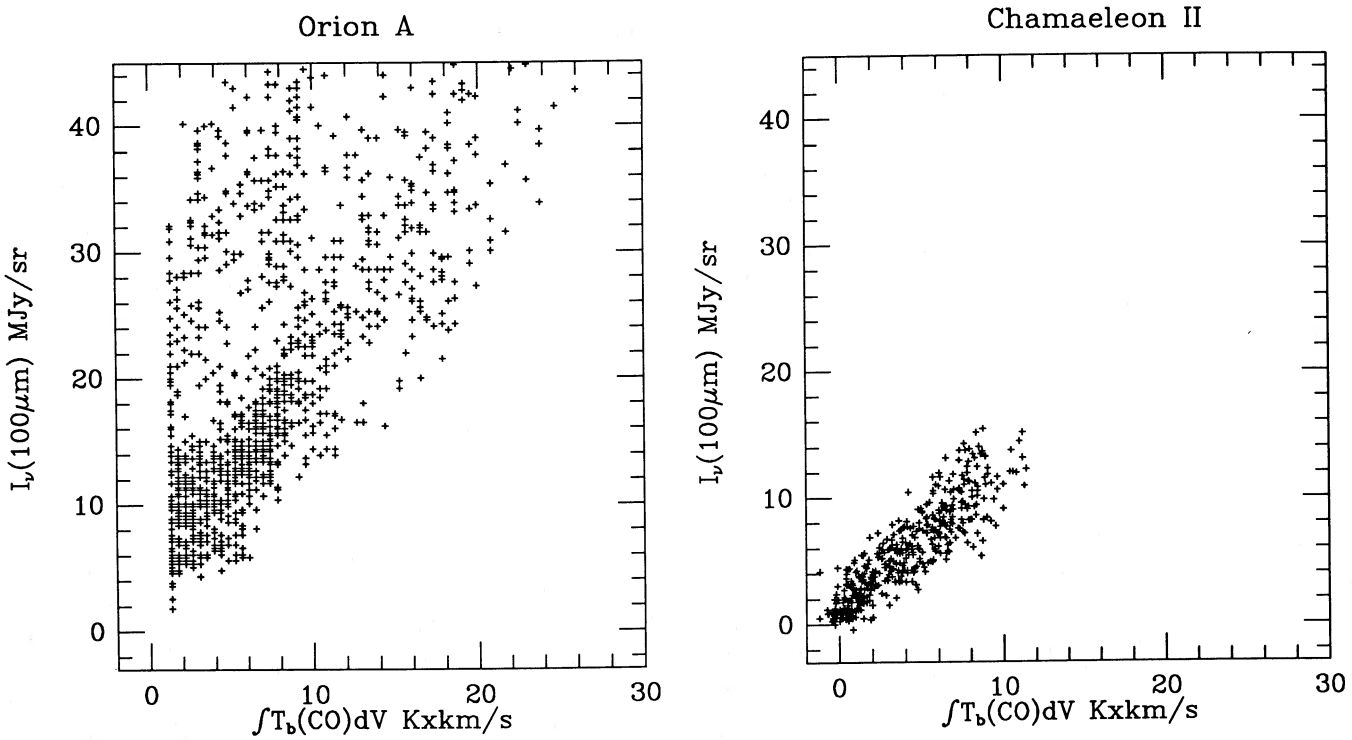

FIG. 11.—Pixel-by-pixel comparison between 100 μm brightness and CO-integrated emission for the Orion A and Chamaeleon II clouds. Each cross represents a 8′ × 8′ pixel. Note that the Orion diagram does not show the full dynamical range of 100 μm brightness in the cloud: in the warm parts of the cloud I_ν(100 μm) is much larger than 45 MJy sr^{-1}.

TABLE 5

INFRARED COLORS OF NEARBY MOLECULAR CLOUDS

Cloud	$I_\nu(12\ \mu m)/I_\nu(100\ \mu m)$	$I_\nu(25\ \mu m)/I_\nu(100\ \mu m)$	$I_\nu(60\ \mu m)/I_\nu(100\ \mu m)$
Chamaeleon I	<0.0031	0.013	0.06
Chamaeleon II	0.013	0.017	0.07
Lupus, Northern Cloud	0.067	0.10	0.20
Ophiuchus, Main Cloud	0.037	0.040	0.26
Ophiuchus, Northern Cloud	0.064	0.065	0.23
Orion A	0.034	0.056	0.21
RCra	0.055	0.078	0.23
Taurus	0.030	0.050	0.16

NOTE.—These colors are average values for large sections of the clouds away from internal heating sources. For the Chamaeleon clouds we achieved a better sensitivity than did the Sky Flux Images (*IRAS Explanatory Supplement* 1985) by averaging scans and crossing the clouds with similar position angles within a 30′ window in the cross-scan direction. Error bars on these colors are typically 20% for the 12/100 μm and 25/100 μm ratios and 10% for the 60/100 μm ratio.

al. (1988*b*). Outside regions of star formation they found ratios between 100 μm and CO fluxes in the range 0.7–2.5 MJy sr^{-1} (K km s^{-1})$^{-1}$; for the purpose of estimating the contribution of molecular clouds to the infrared emission of the solar neighborhood, we use their average value of 1.4 MJy sr^{-1} K^{-1} km^{-1} s. Applying the same bolometric correction as for the high–Galactic latitude emission (Table 2), we get a total infrared emission per unit of CO brightness of 1.0×10^{-6} W m^{-2}(K km s^{-1})$^{-1}$, or 2.5 $L_\odot$ pc^{-2}(K km s^{-1})$^{-1}$; for a ratio between N_{H_2} and CO–integrated brightness of 2.5×10^{20} cm^{-2}(K km s^{-1})$^{-1}$ (Bloemen *et al.* 1986) this last ratio corresponds to an L_{IR}/M_{H_2} ratio of 0.6 $L_\odot/M_\odot$. Dame *et al.* (1987) estimated the density of molecular hydrogen within 1 kpc of the Sun to be 1.3 $M_\odot$ pc^{-2} by summing the masses of the observed molecular clouds; according to the analysis of Bronfman *et al.* (1988) the solar ring (9–10 kpc) value of the H_2 surface density derived from the Galactic CO surveys is slightly higher: 1.7 $M_\odot$ pc^{-2} for their data and, with the same N_{H_2}/W_{CO} calibration, 3 $M_\odot$ pc^{-2} for the data of Sanders, Scoville, and Solomon (1985). Scaling these surface densities by the infrared-luminosity–to–mass-of-gas ratio we derive an infrared luminosity per unit surface in the range 0.8–1.8 $L_\odot$ pc^{-2}. This number does not include the emission from warm regions of molecular clouds associated with massive stars. However, these warm regions account for a nonnegligible fraction of the CO luminosity of the solar neighborhood. For example, in the case of Orion A about one-third of the CO luminosity of the cloud comes from regions with a high infrared-luminosity–to–mass-of-gas ratio (§ IV*d*). Applying this correction factor we estimate the infrared luminosity per unit surface from cold molecular clouds to $\sim 1\ L_\odot$ pc^{-2}.

V. EMISSION FROM H II REGIONS

The knowledge of the distribution of ionizing stars in the solar neighborhood is used to estimate the overall emission from H II regions.

Garmany, Conti, and Chiosi (1982) have compiled a catalog of O stars complete to a distance of 2.5 kpc, from which they derived the average density of ionizing stars in the vicinity of the Sun; note, however, that the stars are not uniformly distributed around the Sun: about two-thirds of the stars cataloged by Garmany Conti, and Chiosi are located within the solar circle. Using their results, and the stellar production rates of Lyman-continuum photons computed by Kurucz (1979) and tabulated by Gusten and Mezger (1983), we obtain for stars more massive than 20 $M_\odot$ a total production rate of Lyman-continuum photons, N_{Lyc}, of 1.7×10^{44} s^{-1} pc^{-2}; the contribution of stars less massive than 20 $M_\odot$ is negligible. Mezger (1978) estimated that in the solar neighborhood $\sim$30% of the Lyman-continuum photons either escape the galaxy or are absorbed by dust, which implies that the rate of Lyman-continuum photons absorbed by gas is $N_{Lyc}' = 1.2 \times 10^{44}$ s^{-1} pc^{-2}; this number is in reasonable agreement with the solar ring (9–10 kpc) value of 1.6×10^{44} s^{-1} pc^{-2} derived from Galactic radio-continuum surveys by Gusten and Mezger.

The infrared luminosity of H II regions is often compared to the Lyman-alpha luminosity defined as the product of the rate of recombinations by the energy of a Lyman alpha photon (Mezger 1978); the radio between the infrared and Lyman-alpha luminosity is referred to as the Infrared excess (IRE). Myers *et al.* (1986) inferred from an extensive study of H II region–molecular cloud associations that the median IRE of the Galactic H II region is 6. Using this value for the H II regions in the solar neighborhood we find an overall luminosity per unit surface of 3.0 $L_\odot$ pc^{-2}. The contribution of H II regions to the infrared luminosity of the solar neighborhood can also be estimated by assuming that Orion is representative of the average properties of nearby OB associations. For the Orion OB I association, the rate of Lyman-continuum photons is $\sim 3.7 \times 10^{49}$ s^{-1}, and the luminosity of associated molecular clouds and H II regions is $10^6\ L_\odot$. Scaling the surface density of production of Lyman-continuum photons, 1.7×10^{44} s^{-1} pc^{-2}, by the Orion ratio between infrared luminosity and ionization rate we get a luminosity per unit surface of 4.6 $L_\odot$ pc^{-2}, 50% higher than our first estimate.

The IRE of an H II region depends on the volume over which the emission is integrated because a substantial fraction of the infrared emission associated with an OB association is radiated by dust outside the region of ionization (Leisawitz 1986). The median IRE of 6 given by Myers *et al.* includes the emission of the molecular clouds associated with the H II regions and does not refer to the H II regions alone. Consequently, the luminosity of 3 $L_\odot$ pc^{-2} represents the emission of H II regions and the associated molecular clouds. The study of the Orion region presented in Appendix C shows that the IRE is even higher if one assigns to the H II regions all of the emission coming from the sphere of influence of the OB association, defined as the volume over which the radiation from the association dominates the ISRF.

VI. ORIGIN OF THE INFRARED EMISSION

a) Solar Neighborhood

To interpret the infrared emission of galaxies in terms of star-formation properties, one must answer two related questions:

1. What are the relative contributions of stars of different type and age to the heating of dust?

2. What are the respective contributions of molecular clouds, atomic gas, and H II regions to the infrared emission?

Attempts to answer these questions from observations of the Galactic plane (Cox, Krugel, and Mezger 1986; Paper II, and references therein) are hampered by confusion because the infrared emission arises in different components of the interstellar medium integrated along the line of sight and by extinction which obscures the distribution of starlight across the Galaxy. In the solar neighborhood, the question of the origin of the infrared emission can be addressed more directly, because the different components of the interstellar medium are observed separately and also because the distribution of stars is known.

In the three preceding sections we have estimated the emission coming from the different components of the interstellar medium. Summing the contributions of atomic gas (9 $L_\odot$ pc^{-2}), molecular clouds (~ 1 $L_\odot$ pc^{-2}), and H II regions (~ 4 $L_\odot$ pc^{-2}) we get a total infrared luminosity per unit surface of 14 $L_\odot$ pc^{-2}. Dust associated with atomic and ionized gas away from star-forming regions accounts for two-thirds of this emission; H II regions and associated molecular clouds contribute $\sim 30\%$; the contribution from molecular clouds, or sections of molecular clouds, not heated by massive stars (cold molecular clouds) is small. These numbers show that 70% of the infrared emission from the solar neighborhood comes from dust, in atomic gas and cold molecular clouds, heated by the ISRF. Using the extinction curve, albedos, and the radiation field tabulated by Mathis, Mezger, and Panagia (1983), we computed that ultraviolet ($0.0912\ \mu\text{m} < \lambda < 0.346\ \mu\text{m}$), optical ($0.346\ \mu\text{m} < \lambda < 0.8\ \mu\text{m}$), and near-infrared photons ($\lambda > 0.8\ \mu\text{m}$) account for 50%, 30%, and 20%, respectively, of the heating of dust by the ISRF. Since ultraviolet photons of the ISRF originate mainly from B stars (Paper II) we find that half of the infrared emission of interstellar matter not associated with star formation comes from stars younger than a few 10^8 yr. Adding this contribution from young stars to the emission of H II regions we estimate that about two-thirds of the infrared emission from the solar neighborhood comes from stars younger than a few 10^8 yr. Therefore, we reach the conclusion that although most of the emission of the solar neighborhood is coming from atomic gas not associated with star formation, about half of the heating of interstellar grains comes from young stars. This result is likely to be valid for most galaxies with a ratio between 100 μm and optical emission comparable to that for the solar neighborhood: νI_ν (100 μm)/νI_ν (0.44 μm) = 0.3 derived from the 100 μm brightness in Table 2 and the blue flux density given by Mathis, Mezger, and Panagia (1983). For other galaxies we obviously expect the fraction of the infrared emission coming from young stars to increase with the ratio between infrared and optical emission.

b) Star-Forming Regions

To investigate how the luminosity of OB associations is spread over the ISM, and to what extent the luminosity of young stars is converted into infrared radiation, we studied in detail the infrared emission of the Orion region.

Data presented in Appendix C lead to the following picture of the Orion region. The OB association with a luminosity of 5×10^6 $L_\odot$ is the main source of radiation over a sphere of 300 pc diameter containing 2.4×10^5 $M_\odot$ of molecular gas and 1.6×10^5 $M_\odot$ of atomic hydrogen. With a total infrared luminosity of 1×10^6 $L_\odot$, molecular clouds and associated H II regions are the dominant sources of the emission; with a luminosity of 4×10^5 $L_\odot$, the H I gas accounts for only 30% of the emission. Therefore, in the 300 pc sphere surrounding the OB association, the origin of the infrared emission is the opposite of what we found in § VI*a* for the whole solar neighborhood. This difference appears clearly if we compare the infrared excess of the Orion region and the solar neighborhood. In Appendix C we estimated the infrared excess of the 300 pc sphere around Orion to 15, while for the solar neighborhood the comparison between the Lyman production rate of 1.2×10^{44} s^{-1} pc^{-2} (§ V) and the infrared luminosity 14 $L_\odot$ pc^{-2} leads to a value of 28. These basic differences prove that the interstellar medium in the close vicinity of OB associations is not the dominant source of infrared emission in the solar neighborhood.

The total infrared emission of the Orion region, $\sim 1.4 \times 10^6$ $L_\odot$, represents only 30% of the luminosity of the OB association; we thus find that a large fraction of the radiation of the association gets spread over an extended volume of the interstellar medium; a study of six OB associations in the outer Galaxy led Leisawitz (1987) to a similar conclusion. Close to the Galactic plane, the average density of the interstellar medium (atomic plus molecular gas) is of the order of 0.6 H atoms cm^{-3} (Lockman 1984; Dame *et al.* 1987). For this density, in the plane, the opacity in the ultraviolet is 2.2 mag kpc^{-1}; however, as the ISM is highly inhomogeneous, the effective opacity is certainly lower. Thus, we estimate that photons can spread as far as 1 kpc from OB associations. As this distance is larger than the scale height of the disk, a significant fraction of the radiation from OB associations leaves the Galaxy. By emphasizing the fact that the radiation of an association of young stars spreads over a wide volume of the Galaxy, the study of Orion strengthens the idea that throughout the interstellar medium a large fraction of the heating of interstellar dust is coming from young stars (§ VI*a*).

The low ratio between infrared and stellar luminosity found in Orion calls into question the use of infrared observations to measure the luminosity of Galactic star-forming regions and the luminosity of young stars in external galaxies. The efficiency of the conversion of stellar luminosity into infrared radiation depends on the density of interstellar matter in and around the star-forming region. As the density of interstellar matter is higher in the molecular ring than in the solar neighborhood, we except the infrared emission to be a better measure of the luminosity of recently formed stars, for star-forming regions in the inner parts of the Galaxy, than for Orion.

VII. INFRARED AND RADIO-CONTINUUM EMISSION

The *IRAS* survey has led to the discovery of a tight correlation between far-infrared and radio-continuum fluxes of spiral and irregular galaxies (de Jong *et al.* 1985; Helou, Soifer, and Rowan-Robinson 1985). *IRAS* observations of the Galaxy and the largest nearby galaxies provide the opportunity to investigate the "microscopic" nature of this correlation by comparing the distribution of the infrared and radio continuum within one galaxy. Adding the brightness at the northern and

southern Galactic poles we get from th survey of Haslam *et al.* (1981) a 408 MHz emission integrated perpendicular to the plane of 25 K; for a spectral index in the range 0.7–0.9, this emission corresponds to a brightness of 0.76 ± 0.1 K at 1420 MHz. Following earlier works we compare the radio-continuum emission with the far-infrared emission defined as the integral of the emission from 40 to 120 μm (see *Cataloged Galaxies and Quasars in the IRAS Survey* 1985); for the high–Galactic latitude spectrum (Table 2) the far-infrared emission represents 41% of the total infrared emission. Thus, the infrared luminosity per unit surface of 14 $L_\odot$ pc^{-2} (§ VI*a*) implies a far-infrared brightness (F_{IR}) of 1.9×10^{-7} W m^{-2} sr^{-1}. Following Helou, Soifer, and Rowan-Robinson (1985), we computed the ratio between flux densities in the far-infrared and at 21 cm:

$$q = \log (F_{IR}/3.75 \times 10^{12} \text{ Hz}/S_{21\text{ cm}}) ,$$

where 3.75×10^{12} Hz is the frequency at 80 μm; we get for the solar neighborhood a value of 2.03 ± 0.06, which is within the scatter of individual galaxies, $q = 2.14 \pm 0.14$ (Helou, Soifer, and Rowan-Robinson 1985).

A similar comparison was made in Orion by integrating the radio and infrared emission in an aperture of 30° (300 pc at a distance of 500 pc) around the Trapezium Stars. The thermal emission from the H II regions was subtracted from the 408 MHz flux which was then converted to 21 cm. For a non-thermal spectral index between 0.7 and 0.9, we found $q = 2.8 \pm 0.06$, a value 6 times higher than the average value for the solar neighborhood. This difference shows that the infrared emission is more concentrated around star-forming regions than the nonthermal radio-continuum emission. In that sense the Orion analysis proves that the infrared–radio-continuum correlation breaks on the scale of a few 100 pc around a region of star formation. Without questioning the idea that cosmic rays are accelerated in star-forming regions, this result indicates that electrons diffuse further away from star-forming regions than do the ultraviolet photons. The infrared and radio-continuum emission also differ in their distribution perpendicular to the plane of the Galaxy (Beuermann, Kanbach, and Berkhuijsen 1986; Paper II).

VIII. DUST PROPERTIES

a) Emission at 12 μm

The spectrum of Table 2 indicates that the emission between 7 and 35 μm represents 40% of the power radiated by dust shortward of 120 μm; this mid-infrared emission accounts for ~25% of the starlight energy absorbed by grains (§ III*g*). Since large grains heated by the local ISRF have an equilibrium temperature much too low (Draine and Lee 1984) to account for any significant emission at these wavelengths, the mid-infrared emission from the nearby interstellar medium (Sellgren, Werner, and Dinnerstein 1983; Boulanger, Baud, and van Albada 1985; Leene 1986), and from the Galaxy (Price 1981; Pajot *et al.* 1986) is considered as strong evidence for the existence of very small grains briefly heated to high temperatures each time they absorb a single photon (Andriesse 1978; Sellgren 1984; Puget, Léger, and Boulanger 1985). Studies of individual objects indicate that the ratio between mid- and far-infrared emission varies from place to place in the solar neighborhood (Ryter, Puget, and Pérault 1987); however, the high–Galactic latitude cosecant laws demonstrate that on average a significant fraction of the emission of interstellar dust is radiated in the mid-infrared, and consequently that very small grains are a pervasive component of interstellar dust.

Infrared spectra from 2 to 13 μm of two reflection nebulae (NGC 2023 and 7023; Sellgren *et al.* 1985) show that most of the emission observed in the 12 μm band of *IRAS* is associated with the infrared features at 7.7, 8.8, and 11.3 μm (Puget 1987); adding the contribution of the 3.3 and 6.2 μm features, we find that more than half of the emission from the reflection nebulae in the 2–15 μm band comes from features which Léger and Puget (1984) identified with polycyclic aromatic hydrocarbon molecules (PAHs). At high–Galactic latitude, the emission in the 12 μm band of *IRAS* is 5.5×10^{-32} W per hydrogen atom. Assuming that NGC 2023 and NGC 7023 are representative of the average properties of the nearby interstellar medium we derive from the 12 μm flux a total emission in the range of wavelengths 2–15 μm of the order of 1.5×10^{-31} W (H atom)$^{-1}$. We assume that most of this emission comes from PAHs, and use the integrated flux to estimate the average abundance of PAHs in the nearby interstellar medium. Absorption cross sections in the ultraviolet and visible have been measured by Léger and d'Hendecourt (1987) for a mixture of many different PAHs; assuming that the molecules studied by Léger and d'Hendecourt are representative of interstellar PAHs, Encrenaz *et al.* (1987) estimated that PAHs absorb from the local ISRF $\sim 2.4 \times 10^{-27}$ W per atom of carbon. Comparing this number with the emission in the 2–15 μm band of 1.5×10^{-31} W (H atom)$^{-1}$, we derive an abundance of carbon in PAHs of 4×10^{-5} per H atom, which represents ~15% of the cosmic abundance of carbon. Since part of the energy absorbed by PAHs is radiated through optical fluorescence (Allamandola, Tielens, and Barker 1985; Omont 1986), this estimate must be considered as a lower limit.

b) Emission at 25, 60, and 100 μm

At $|b| > 10°$ the cosecant laws give an average ratio between 100 μm and H I emission, $I_\nu(100\ \mu\text{m})/N_H$, of 0.85 MJy sr^{-1} ($10^{20}$ H atoms)$^{-1}$ cm^2 (Table 4). This value is in good agreement with the calculations of Draine and Lee (1984) on the basis of the graphite-silicate dust model proposed by Mathis, Rumpl, and Nordsieck (1977). However, the same model fails to reproduce the $I_\nu(60\ \mu\text{m})/I_\nu(100\ \mu\text{m})$ color of 0.21 by a factor of 2. A possible explanation of this discrepancy was suggested by Draine and Anderson (1985): a large fraction of the 60 μm emission could result from temperature fluctuations in the smallest grains; a large contribution from small grains to the 60 μm emission could also explain why in the infrared–H I correlations presented in § III*b* the 60/100 μm color does not depend significantly on the 100 $\mu\text{m}/N_H$ ratio.

The effects of temperature fluctuations on infrared spectra have been investigated by Draine and Anderson for several mixtures of graphite and silicate grains with different degrees of enhancement in small grains. One of their models does reproduce well the observed 25/100 μm and 60/100 μm colors of the high–Galactic latitude spectrum, but it assumes that 19% of the cosmic abundance of carbon is in graphite grains smaller than 50 Å which is inconsistent with the average extinction curve of the local interstellar medium. This result suggests that besides the 12 μm emission a significant number of small grains is necessary to explain the 25 and 60 μm emission of the local interstellar medium; however, the nature of these small grains is still unclear: are they aggregates of PAHs, or are they made of other elements?

IX. SUMMARY

The large-scale study of the infrared emission from the solar nieghborhood presented in this paper leads to the following conclusions:

1. *IRAS* observations show the existence of Galactic emission at $|b| > 10°$ at 12, 25, 60, and 100 μm. This emission comes mainly from dust heated by the radiation field of the Galaxy, associated with atomic gas, and possibly diffuse ionized gas.

2. Away from heating sources, and outside dense condensations in molecular clouds ($A_v > 3$ mag) the 60 and 100 μm emission of the nearby ISM is well correlated with the column density of gas on scales smaller than a few hundred parsecs; on larger scales, the ratio between infrared emission and gas column density varies significantly from one region to another. The variations in the infrared emission per H atom are probably related to changes in the intensity of the ISRF. Away from OB associations, we find for the H I gas an average infrared-luminosity–to–mass-of-neutral-atomic-gas ratio of 1.9 $L_\odot/M_\odot$; part of this emission could come from dust associated with diffuse ionized gas.

3. From $|b| = 20°$–$90°$ the latitude distribution of the H I emission, scaled by the ratio of 100 μm to H I brightness measured at $|b| > 50°$, agrees very closely with the latitude distribution of the 100 μm emission. We see two possible explanations to the fact that these two profiles differ by much less than the expected contribution of diffuse ionized gas: (*a*) the diffuse ionized gas is deficient in dust, (*b*) The distribution of the ionized gas is correlated with the distribution of the H I gas.

4. The good correlation between infrared emission and gas column density implies that *IRAS* data can be used to study the distribution of molecular and atomic gas away from the Galactic plane, and to measure the extinction at high Galactic latitude. For relative measurements over angular scales smaller than typically 10°, the sensitivity limit at 100 μm corresponds to emission from a column density of gas of a few 10^{19} H atoms cm^{-2} or A_v of 0.01 mag.; uncertainties on absolute measurements of A_v are of the order of 0.05 mag. The median extinction in the polar caps ($|b| > 50°$) is $A_v = 0.10^{+0.06}_{-0.03}$ mag.

5. After subtraction of the Galactic and zodiacal light, we find at 100 μm a residual background of 1.8 MJy sr^{-1}; this number could be somewhat lower if there is any Galactic emission from dust associated with ionized gas in the H I holes at high latitude (see Appendix B). This background could be of extragalactic origin. However, there are two other possible explanations for this emission: (1) the zodiacal light at high ecliptic latitude does not follow a cosecant law, and there is an error in the zero level of the zodiacal light subtraction (Appendix A, § III*c*); (2) the calibration of the zero level of the 100 μm data is uncertain by a number comparable to, or greater than, the measured background.

6. On average, embedded stars have a negligible contribution to the infrared emission of molecular clouds not associated with H II regions. Those clouds which account for a large fraction of the molecular mass in the Galaxy are mainly heated by the ISRF. In the solar neighborhood, they have an infrared-luminosity–to–mass-of-molecular-hydrogen-ratio of the order of 0.6 $L_\odot/M_\odot$, one-third of the value measured for the atomic gas. The difference between atomic and molecular gas is due to the optical depth of molecular clouds to ultraviolet and optical photons from the ISRF.

7. A global budget of the infrared emission from the solar neighborhood shows that stars younger than a few 10^8 yr contribute for two-thirds of the infrared luminosity of dust although most of the infrared emission from the solar neighborhood comes from interstellar matter not associated with current star formation. This result is supported by a study of Orion which shows that the luminosity of OB associations spreads over large volumes of the interstellar medium. The use of infrared observations to measure the overall luminosity of star-forming regions in the Galaxy is questioned by the fact that a small fraction of the luminosity of young stars is locally converted into infrared radiation.

8. The ratio between the overall infrared and radio-continuum emission from the solar neighborhood is close to the average value found for galaxies. Comparing infrared and radio-continuum data over a 30° region around Orion we find a value for this ratio 5 times higher than the average value of the solar neighborhood. This difference shows that the infrared–radio-continuum correlation observed among galaxies breaks down on the scale of a few hundred parsecs around regions of star formation.

9. On average, at $|b| > 10°$ we find that the emission in the 7–35 μm band accounts for 40% of the emission of interstellar dust shortward of 120 μm and 25% of the stellar energy absorbed by dust. Since large grains heated by the local ISRF have an equilibrium temperature much too low to account for any significant emission in this range of wavelengths, this result demonstrates that grains small enough to be transiently heated to temperatures of several hundred degrees when they absorb a single photon, are a pervasive component of interstellar dust. Assuming that the 12 μm emission comes from polycyclic aromatic hydrocarbons, we find that these molecules account for $\sim$15% of the cosmic abundance of carbon. A larger number of large molecules or small grains is necessary to explain the 25 μm emission, and possibly about half of the 60 μm emission from the interstellar medium.

We are particularly indebted to J. L. Puget, whose pioneering ideas have inspired most of this work, and C. Beichman for his tireless efforts to motivate numerous improvements in the manuscript. We are grateful to M. Hauser, G. Helou, G. Neugebauer, and T. Soifer for useful comments on early drafts of this paper. This work benefited from discussions with F. X. Désert, P. Hacking, and F. Viallefond. We would like to thank A. A. Stark for providing us with the H I survey of the Bell Laboratories prior to publication; a Galactic map of the emission integrated in velocity was kindly made available to us by D. N. Burrows and F. X. Désert. We thank J. Vrtilek for his help in the study of the zodiacal light at high ecliptic latitude. This work was done while F. B. held a National Research Council Research Associateship at the Goddard Institute for Space Studies and the Infrared Processing and Analysis Center.

APPENDIX A

ZODIACAL LIGHT SUBTRACTION

I. INTRODUCTION

An accurate separation of the Galactic and zodiacal components of the infrared emission is necessary to use the *IRAS* data to study the zodiacal light at long wavelengths and the emission of Galactic objects on large angular scales. At 12 and 25 μm the zodiacal light dominates the observed emission and must be subtracted with a high accuracy to observe weak residuals associated with Galactic sources; at 100 μm, and to a lesser extent at 60 μm, the Galactic contribution represents a significant fraction of the emission over the whole sky, and the Galactic component needs to be modeled to measure the zodiacal contribution (see Table 6 for a quantitative comparison of Galactic and zodiacal emission). A method of separating zodiacal and Galactic contributions, based on a limited set of assumptions is presented here. This method is described in a general way in § II of this Appendix; its implementation is outlined in § III. Uncertainties in the zodiacal light subtraction are discussed in § IV.

II. MODEL OF ZODIACAL EMISSION

The zodiacal emission depends both on the direction of observation and its position with respect to the Sun. If we study separately scans for which the ecliptic latitude increases and decreases with time (respectively, ascending and descending scans), the zodiacal emission can be written as a function of three variables: the time of observation t, the elongation of the scan e (angle between the direction of observation and the Sun), and the ecliptic latitude β. We assume that the zodiacal light varies smoothly with time and elongation. Then, within a reasonable range of elongation and time, the zodiacal emission at a given ecliptic latitude can be approximated by a linear function of time and elongation; by averaging *IRAS* measurements within this range of elongation and time, we get

$$\langle \mathrm{DATA} \rangle = \langle \mathrm{ZE} \rangle + \langle \mathrm{GAL} \rangle = \mathrm{ZE}(\langle e \rangle, \langle t \rangle, \beta) + \langle \mathrm{GAL} \rangle \, . \tag{A1}$$

In order to derive the zodiacal emission from this equation, we need to be able to estimate or neglect the Galactic term. Within a given range of elongation and time, *IRAS* observed at a given ecliptic latitude a wide segment of positions in the Galaxy. As we do not need to average together all measurements within the range of elongation and time, we have the possibility of selecting the lines of sight in the Galaxy which get used to measure the zodiacal light. The comparison of infrared and H I data at high Galactic latitude shows that outside molecular clouds the 60 and 100 μm emission are well correlated with the H I emission integrated in velocity. For averaging, we use only positions where the 60 and 100 μm emission are correlated with the H I emission; this sleection criterion enables us to make use of the H I data to compute the Galactic term in the right-hand side of equation (A1). At 12 and 25 μm, the weakness of the Galactic emission with respect to the zodiacal emission prevents the study of the correlation between infrared and H I emission, independently of the subtraction of the zodiacal light. Therefore, we simply assume that above some Galactic latitude and outside strong sources the Galactic emission is negligible. The identification of regions where infrared and H I emission are correlated, and the localization of strong point sources is done through an iterative procedure. To compute the first model of the zodiacal light we exclude all measurements close to the Galactic plane; the results of the first subtraction are then used to localize in a systematic way point sources and regions of bad correlation between infrared and H I emission which can be excluded from the data averaging for the computation of the second model. This process can be iterated as many times as necessary.

III. IMPLEMENTATION

The method described in § II of this Appendix can be implemented in different ways and the options taken here are not necessarily optimal.

a) Data Averaging

The *IRAS* data taken from the Zodiacal History File (*IRAS Explanatory Supplement* 1985) were averaged in intervals of 5° in elongation, and 50 days in time centered every 2.5 and 25 days. At the first iteration, all data points within 25° of the Galactic plane or in the Magellanic clouds are excluded from the averaging process. For the second iteration we excluded data points for which the 12 μm emission after zodiacal light subtraction is larger than 1.5 MJy sr^{-1} and those where the 100 μm after subtraction of the zodiacal light and the emission associated with the H I gas was larger than 8 MJy sr^{-1}; for the subtraction of the emission

TABLE 6

COMPARISON OF GALACTIC AND ZODIACAL EMISSION

	ZODIACAL LIGHT ELONGATION 90°		GALACTIC EMISSION AVERAGED OVER LONGITUDES	
	$\beta = 0°$	$\beta = 90°$	$\lvert b \rvert < 2°$	$b = 90°$
12 μm.....	40.	14.	6.	0.05
25 μm.....	85.	28.	10.	0.08
60 μm.....	28.	7.	30.	0.2
100 μm.....	10.	2.	130.	1.

NOTE.—These numbers are approximate values which allow a quick estimate of the relative intensities of the zodiacal and Galactic emission at the different wavelengths of the *IRAS* observations. Values are in MJy sr^{-1}.

associated with the H I gas we used a uniform $I_\nu(100\ \mu m)/N_H$ ratio of 0.8 MJy sr^{-1}/(10^{20} H atoms cm^{-2}). The 12 μm selection criterion excludes data in the direction of bright infrared stars; the 100 μm criterion is designed to exclude regions like molecular clouds and H II regions where infrared and H I emission do not correlate.

The H I emission integrated over velocities is averaged in the same way as the infrared data was, as if *IRAS* had a fifth set of detectors which had measured this integrated emission. After averaging, the amplitude of the H I emission is typically a few hundred K km s^{-1}. This value implies that the Galactic term in equation (A1) is of the order of 0.1–0.2 MJy sr^{-1} at 12 and 25 μm, 1 MJy sr^{-1} at 60 μm, and a few MJy sr^{-1} at 100 μm. The averaged H I emission is subtracted from the averaged 60 and 100 μm emission using $I_\nu(60\ \mu m)/N_H$ and $I_\nu(100\ \mu m)/N_H$ ratios of 0.16 and 0.8 MJy sr^{-1} for 10^{20} H atoms cm^{-2} sr^{-1}. We estimate that this subtraction removes the Galactic emission within a few tenths MJy sr^{-1} at 60 μm and 0.5 MJy sr^{-1} at 100 μm.

b) *Model of the Zodiacal Light*

The averaged data corrected for Galactic emission are used to determine the variation of the zodiacal emission with ecliptic latitude (zodiacal emission profile) on a grid with regular spacings in elongation and time. Due to the galaxy exclusion and a nonuniform distribution of scans in a given interval of elongation and time, the data-averaging process provides the zodiacal emission for a nonuniformly distributed set of elongations and times. To interpolate the results of the data averaging onto a regularly spaced grid, we used rough estimates of the local derivatives of the zodiacal emission with respect to elongation and time. The elongation derivative was assumed independent of time and was measured for each ecliptic latitude from a linear fit of the averaged data points versus elongation. After regridding in elongation, we fitted the zodiacal emission at a given elongation and ecliptic latitude with a cosine function of time. These fits are used to interpolate data in time.

Each zodiacal emission profile has a missing segment corresponding to lines of sight close to the Galactic plane. Where the Galactic and ecliptic plane are not coincident, the missing segments in ascending and descending profiles do not overlap. Then we combine the two profiles to fill the missing segments. As ascending and descending profiles differ at a 5% level, it is necessary to adjust the two profiles before we combine them. Profiles are matched with a linear function of ecliptic latitude fitted over a limited set of points at the edges of the missing segment. When this method could not be used because segments of missing data in ascending and descending profiles coincide, the holes in the profiles were filled by interpolation in elongation or time. The missing data segments are the main problem of our subtraction of the zodiacal light. The technique used to fill the holes is not completely satisfactory, and the subtraction of the zodiacal light is significantly less accurate in the Galactic plane than at high Galactic latitude.

c) *Zero Level of the Zodiacal Light Model at 100 μm*

In writing equation (A1) we implicitly assumed that there is no significant contribution from an isotropic background in the *IRAS* data. Within this assumption, if any such background exists it will be subtracted from the data with the zodiacal light. As we want to discuss the possible existence of an extragalactic background at 100 μm, we calibrated the zero level of the 100 μm zodiacal light independently of this assumption. From the Zodiacal History File (*IRAS Explanatory Supplement* 1985) we selected all measurements with a solar elongation in the range 89°–91° at ecliptic latitudes larger than 30°, absolute Galactic latitudes larger than 25°, and in directions where the integrated H I emission in the survey of Stark *et al.* (1987) is lower than 200 K km s^{-1}. The points we selected are clustered in two time intervals of a few days. For both time intervals, the 100 μm data points are well fitted by the following relation:

$$I_\nu(100\ \mu m) = (2.15 \pm 0.15)\,|\sin(\beta)| + 3.3\ \text{MJy sr}^{-1}$$

If we assume that the zodiacal light follows at high ecliptic light a cosecant law, this relation implies that the value of the 100 μm zodiacal light at the north ecliptic pole is 2.15 $\pm$ 0.15 MJy sr^{-1}. We calibrated the zero level of our 100 μm model using this value.

d) *Subtraction of the Zodiacal Emission*

The relative calibration of the gain and the zero level is generally consistent from scan to scan within a few percent. At 12 and 25 μm, these small differences in the calibration need to be corrected because their amplitude is comparable to the Galactic emission we want to measure; we corrected for differences in gain and offset by fitting the zodiacal emission as a lower envelope to the scan. Positions within 15° of the Galactic plane were not used to derive the fit coefficients. No gain and offset corrections were applied to the 60 and 100 μm data. The 100 μm profiles of zodiacal emission which are significantly distorted by Galactic residuals were not used to subtract the zodiacal light from the 100 μm data; we achieved a more accurate subtraction by using the 60 μm profiles scaled by a color ratio $I_\nu(60\ \mu m)/I_\nu(100\ \mu m)$ of 0.371. The zodiacal light along a given scan is computed from the zodiacal emission profiles by linear interpolation in time, elongation, and ecliptic latitude. After subtraction of the zodiacal light, scans are projected onto on all-sky map of the Galactic emission with a resolution of the order of 0°.5. Only scans from the two first coverages of the survey (hours confirmation 1 and 2) were used; scans shorter than 50° or with elongations smaller than 81° or larger than 99° were discarded. Few scans for which the 25 μm data did not correlate well with the zodiacal light (correlation coefficient smaller than 0.96) were also discarded at all wavelengths.

IV. RESULTS

The quality of the subtraction of the zodiacal light was assessed by studying residuals in the polar caps ($|b| > 50°$). Around the Galactic poles the 12 and 25 μm residuals are dominated by errors in the subtraction of the zodiacal light. Therefore, the dispersion of these residuals, 0.11 and 0.18 MJy sr^{-1} at 12 and 25 μm, respectively, represents a good estimate of the accuracy of the subtraction of the zodiacal light away from the Galactic plane; the dispersion corresponds to a few tenths of a percent of the zodiacal emission in the ecliptic plane for an elongation of 90°. Close to the Galactic plane the subtraction is less accurate; errors

can be as large as 1 and 2 MJy sr^{-1} at 12 and 25 μm, respectively. To build the zodiacal model, we assumed that the Galactic contribution to the 12 and 25 μm emission at high latitude is negligible with respect to the zodiacal light. This assumption explains why the cosecant law observed at latitudes smaller than 30° does not extend to the poles. This systematic error adds up to the statistical error given earlier. In the polar caps, the dispersion around the 60 μm–H I correlation is 0.4 MJy sr^{-1}. As the correlation between infrared and H I emission is not necessarily perfect, this number is an upper limit to errors in the subtraction of the zodiacal light at 60 μm; scaling this number by the $I_\nu(60\ \mu\text{m})/I_\nu(100\ \mu\text{m})$ ratio of 0.37 used in subtracting the zodiacal light at 100 μm we get an upper limit of 0.15 MJy sr^{-1} at 100 μm. However, the assumption of a constant color ratio independent of elongation and ecliptic latitude is an additional source of error. By comparing the 100 μm profiles of zodiacal emission derived from the data averaging with the 60 μm profiles scaled by the color ratio of 0.371, we estimated that the additional error is of the order of 0.3 MJy sr^{-1}. Taking into account the different sources of errors we estimate that at high Galactic latitude the subtraction of the 100 μm zodiacal light is accurate to 0.5 MJy sr^{-1}.

APPENDIX B

RESIDUAL BACKGROUND AT 100 MICRONS

Figure 5 shows that the 100 μm and H I emission are well correlated over the polar caps ($|b| > 50°$); a linear regression to the data points in each plot gave a nonzero intercept of 1.8 ± 0.3 MJy sr^{-1}. Linear least-square fits computed separately for the northern and southern polar caps lead to similar values for the intercept, which suggests that this residual emission is isotropic. For an emissivity similar to that for the H I gas we expect the 100 μm emission from ionized gas to be of the order of 0.6 MJy sr^{-1} on average over the polar caps. Then, if there is as much ionized gas in the holes of H I emission as on average at high latitude the residual background is only 1.2 MJy sr^{-1}. This background could be of extragalactic origin (Rowan-Robinson 1986). However, there are two other possible explanations for this emission:

1. The zodiacal light at high ecliptic latitude does not follow a cosecant law, and there is an error in the zero level of the zodiacal light subtraction (see § III*c* of Appendix A).
2. The calibration of the zero level of the 100 μm data described in Hauser *et al.* (1984) and the Supplement is uncertain by a number comparable to, or greater than, the measured background.

APPENDIX C

THE ORION REGION

This Appendix presents data on the luminosity of the Orion OB association, and the interstellar matter in the Orion region, used in § VI*b*, of the main body of this Paper. An average distance of 500 pc is used for all objects in Orion.

On the basis of the stellar catalog of Humphreys (1978), we estimate the total luminosity of stars earlier than B0.5 ($M_* > 18\ M_\odot$), belonging to the Orion OBI association, to be $2.7 \times 10^6\ L_\odot$; ionizing photons account for roughly 10% of this luminosity. To measure the contribution of less massive stars we assume that star formation following a standard initial mass function (IMF) with an upper mass cutoff of 40 $M_\odot$ (O5 star), has been going on in Orion for $\sim 10^7$ yr, the estimated age of the oldest subassociation (Blaauw 1964). Using the IMF given in § IV and the calculation presented in Figure 10, we find that the luminosity of stars later than B0.5 ($M_* < 18\ M_\odot$) is roughly equal to the luminosity of the more massive stars; thus, we assign a total luminosity of 5×10^6 $L_\odot$ to the Orion OBI association. A sphere of 300 pc diameter (30° at the distance of Orion), centered on the Trapezium cluster will include most stars in the association; the OB association maintains in this volume an average density of radiation,

$$u = 3L/(c4\pi R^2) = 0.44\ \text{eV cm}^{-3}\ ,$$

comparable to the average density of radiation in the solar neighborhood, $u = 0.42$ eV cm^{-3} for the ISRF tabulated by Mathis, Mezger, and Panagia (1983). However, the radiation of the OB association which is mainly ultraviolet photons is more efficient in heating the dust than the ISRF.

The 300 pc sphere around the Trapezium includes all of the molecular clouds observed in CO by Maddalena *et al.* (1986) apart from Monoceros R2, the Southern Filament, NGC 2149, and LDN 1653, 4, 5, 6; the total mass of these clouds is $2.4 \times 10^5\ M_\odot$. Using an H I surface density of 5 $M_\odot$ pc^{-2} and the z distribution of Lockman (1984), we computed that the average density of H I in a 300 pc sphere centered at $z = 160$ pc (Trapezium) is 0.25 cm^{-3}. For this density, the total mass of H I in the sphere is $9 \times 10^4\ M_\odot$. However, the H I surveys show a clear excess of H I emission in the Orion region compared to the average Galactic latitude profile; Gordon (1971) estimated this excess to $7 \times 10^4\ M_\odot$, such that the total mass of atomic gas in the 300 pc sphere is $1.6 \times 10^5\ M_\odot$. Finally, we are led to the following picture of the Orion region. The OB association with a luminosity of $5 \times 10^6\ L_\odot$ is the main source of radiation over a sphere of 300 pc diameter containing $4 \times 10^5\ M_\odot$ of gas out of which 60% is molecular.

The infrared luminosity of the molecular clouds and associated H II regions is $1 \times 10^6\ L_\odot$; 60% of this luminosity comes from the Orion A and B nebulae alone (Boulanger *et al.* 1988*b*). The results of the infrared–H I correlation in Orion (§ III*c*) give for the Orion region a L_{IR}/M_H of $2.5\ L_\odot/M_\odot$; using this number we estimate the infrared luminosity of the atomic gas to be $4 \times 10^5\ L_\odot$. The total infrared luminosity of the Orion region, $1.4 \times 10^6\ L_\odot$ represents only 20% of the luminosity of the OB association. The ratio between infrared luminosity and mass of gas is for the whole sphere $3.6\ L_\odot/M_\odot$, a number slightly higher than the one derived for the H I gas alone. Reich (1978) estimated the total thermal radio-continuum flux density of Orion to be 1115 ± 140 Jy at 21 cm

(~400 Jy for Orion A, 110 Jy for Orion B, 185 Jy for λ Orionis, and 420 Jy for the Barnard Loop). Comparing this thermal flux with the infrared emission, we get an infrared emission of 15 for the whole 300 pc sphere, and 11 if we only take into account the infrared emission from molecular clouds and H II regions. The radio flux implies that the number of Lyman-continuum photons absorbed by hydrogen atoms is 2.2×10^{49} s^{-1}; from the stellar catalog of Humphreys (1978) we estimate the total production rate of Lyman-continuum photons to be 3.7×10^{49} s^{-1}.

REFERENCES

Allamandola, L. J., Tielens, A. G. G. M., and Barker, J. R. 1985, *Ap. J.* (*Letters*), **290**, L25.
Andriesse, C. D. 1978, *Astr. Ap.*, **66**, 169.
Beuermann, K., Kanbach, G., and Berkhuijsen, E. M. 1986, *Astr. Ap.*, **153**, 17.
Blaauw, A. 1964, *Ann. Rev. Astr. Ap.*, **2**, 213.
Bloemen, J. B. G. M., Strong, A. W., Blitz, L., Cohen, R. S., Dame, T. M., Grabelsky, D. A., Hermsen, W., Lebrun, F., Mayer-Hasselwander, H. A., and Thaddeus, P. 1986, *Astr. Ap.*, **154**, 25.
Bohlin, R. C., Savage, B. D., and Drake, J. F. 1978, *Ap. J.*, **224**, 132.
Boulanger, F., Baud, B., and van Albada, G. D. 1985, *Astr. Ap.*, **144**, L9.
Boulanger, F., Beichman, C., Désert, F. X., Helou, G., Pérault, M., and Ryter, C. 1988*a*, *Ap. J.*, in press.
Boulanger, F., Cohen, R. S., Gaida, M., Grenier, I., Koprucu, M., Maddalena, R. J., Thaddeus, P., and Ungerechts, H. 1988*b*, in preparation.
Bronfman, L., Cohen, R. S., Alvarez, H., May, J., and Thaddeus, P. 1988, *Ap. J.*, **324**, 248.
Cataloged Galaxies and Quasars Observed in the IRAS Survey. 1985, prepared by C. J. Lonsdale, G. Helou, J. C. Good, and W. Rice (Jet Propulsion Laboratory).
Caux, E., Puget, J. L., Serra, G., Gispert, R., and Ryter, C. 1985, *Astr. Ap.*, **144**, 37.
Cernicharo, J., and Guélin, M. 1987, *Astr. Ap.*, **176**, 299.
Colomb, F. R., Poppel, W. G. L., and Heiles, C. 1980, *Astr. Ap. Suppl.*, **40**, 47.
Cox, P., Krugel, E., Mezger, P. G. 1986, *Astr. Ap.*, **155**, 380.
Cox, P., and Leene, A. 1987, *Astr. Ap.*, **174**, 203.
Dame, T. M., Ungerechts, R. S., Cohen, R. S., de Geus, E., Grenier, I. A., May, J., Murphy, D. C., Nyman, L. A., and Thaddeus, P. 1987, *Ap. J.*, **322**, 706.
de Jong, T., Klein, U., Wielebinski, R., and Wunderlich, E. W. 1985, *Astr. Ap.*, 147, L6.
de Vaucouleurs, G., and Buta, R. 1983, *A.J.* **88**, 939.
de Vries, C. P., and Le Poole, R. S. 1985, *Astr. Ap.*, **145**, L7.
de Vries, H. W., Heithausen, A., and Thaddeus, P. 1987, *Ap. J.*, **319**, 723.
Draine, B. T., and Anderson, N. 1985, *Ap. J.*, **292**, 494.
Draine, B. T., and Lee, H. M. 1984, *Ap. J.*, **285**, 89.
Encrenaz, T., Puget, J. L., Bibring, J. P., Combes, M., Crovisier, J., Emerich, C., d'Hendecourt, L., Rocard, F. 1987, *Astr. Ap.*, in press.
Flannery, B. P., Roberge, W., and Rybicki, G. B. 1980, *Ap. J.*, **236**, 598.
Garmany, C. D., Conti, P. S., and Chiosi, C. 1982, *Ap. J.*, **263**, 277.
Gordon, C. P. 1971, *A.J.*, **75**, 914.
Ghosh, S. K., Drapatz, S., and Peppel, U. C. 1986, *Astr. Ap.*, **167**, 341.
Gusten, R., and Mezger, P. G. 1983, *Vistas Astr.*, **26**, 159.
Hacking, P., and Houck, J. R. 1987, *Ap. J. Suppl.*, **63**, 311.
Harding, D. S., and Harding, A. K. 1982, *Ap. J.*, **257**, 603.
Haslam, C. G. T., Salter, C. J., Stoffel, H., and Wilson, W. E. 1981, *Astr. Ap. Suppl.*, **47**, 1.
Hauser, M. H., *et al.* 1984, *Ap. J.* (*Letters*), **278**, L15.
Heiles, C., and Habing, H. J. 1974, *Astr. Ap. Suppl.*, **14**, 1.
Helou, G., Soifer, B. T., and Rowan-Robinson, M. 1985, *Ap. J.* (*Letters*), **298**, L7.
Helou, G. 1986, *Ap. J.* (*Letters*), **311**, L33.
Henderson, A. P., Jackson, P. D., and Kerr, F. J. 1982, *Ap. J.*, **263**, 182.
Humphreys, R. M. 1978, *Ap. J. Suppl.*, **38**, 309.
IRAS Explanatory Supplement. 1986, ed. C. A. Beichman, G. Neugebauer, H. J. Habing, P. E. Clegg, and T. J. Chester (Washington: GPO).
Kulkarni, S. R., and Heiles, C. 1986, in *Galactic and Extragalactic Radio Astronomy*, ed. K. I. Kellerman and G. L. Verschuur (New York: Springer-Verlag).
Kurucz, R. L. 1979, *Ap. J. Suppl.*, **40**, 1.
Leene, A. 1986, *Astr. Ap.*, **154**, 295.
Léger, A., and d'Hendecourt, L. B. 1987, in preparation.
Léger, A., Puget, J. L. 1984, *Astr. Ap.*, **137**, L5.
Leisawitz, D. 1987, *Star Formation in Galaxies*, ed. C. J. Lonsdale Persson (Washington: GPO).
Lequeux, J. 1979, *Astr. Ap.*, **80**, 35.
Lockman, F. J. 1984, *Ap. J.*, **283**, 90.
Lockman, F. J., Jahoda, K., and McCammon, D. 1986, *Ap. J.*, **302**, 432.
Low, F. J., *et al.* 1984, *Ap. J.* (*Letters*), **278**, L19.
Maddalena, R. J., Morris, M., Moscowitz, J., and Thaddeus, P. 1986, *Ap. J.*, **303**, 375.
Magnani, L. Blitz, L., and Mundy, L. 1985, *Ap. J.*, **295**, 402.
Mathis, J. S., Rumpl, W., and Nordsieck, K. H. 1977, *Ap. J.*, **217**, 425.
Mathis, J. S., Mezger, P. G., and Panagia, N. 1983, *Astr. Ap.*, **128**, 212.
Mezger, P. G. 1978, *Astr. Ap.*, **70**, 565.
Miller, G. E., and Scalo, J. M. 1978, *Ap. J. Suppl.*, **41**, 513.
Myers, P. C., Dame, T. M., Thaddeus, P., Cohen, R. S., Silverberg, R. F., Dwek, E., and Hauser, M. G. 1986, *Ap. J.*, **301**, 398.
Omont, A. 1986, *Astr. Ap.*, **169**, 159.
Natta, A., and Panagia, N. 1984, *Ap. J.*, **287**, 228.
Pajot, F., Boissé, P., Gispert, M., Lamarre, J. M., Puget, J. L., and Serra, G. 1986, *Astr. Ap.*, **157**, 393.
Pérault, M., Boulanger, F., Puget, J. L., and Falgarone, E. 1987, *in preparation* (Paper II).
Phillipps, S., Kearsey, S., Osborne, J. L., Haslam, C. G. T., and Stoffel, H. 1981, *Astr. Ap.*, **103**, 405.
Price, S. 1981, *A.J.*, **86**, 193.
Puget, J. L. 1985, *Birth and Infancy of Stars*, ed. R. Lucas, A. Omont, and R. Stora (Elsevier Science Publishers), p. 77.
Puget, J. L. 1987, *Polycyclic Aromatic Hydrocarbons*, eds. A. Léger, L. d'Hendecourt, and N. Bocarra (Dordrecht: Reidel), p. 303.
Puget, J. L., Léger, A., and Boulanger, F. 1985, *Astr. Ap.*, **142**, L19.
Reich, W. 1978, *Astr. Ap.*, **64**, 407.
Reynolds, R. J. 1984, *Ap. J.*, **282**, 191.
Rowan-Robinson, M. 1986, *Light on Dark Matter*, ed. F. P. Israel, (Dordrecht: Reidel), p. 499.
Ryter, C., Puget, J. L., and Pérault, M. 1987, *Astr. Ap.*, **186**, 312.
Sandage, A. 1973, *Ap. J.*, **183**, 711.
Sanders, D. B., Scoville, N. Z., and Solomon, P. M. 1985, *Ap. J.*, **289**, 373.
Scalo, J. M. 1986, *Fund. Cosmic Phys.*, **11**, 1.
Sellgren, K. 1984, *Ap. J.*, **277**, 623.
Sellgren, K., Allamandola, L. J., Bregman, J. D., Werner, M. W., and Wooden, D. H. 1985, *Ap. J.*, **299**, 416.
Sellgren, K., Werner, M. W., and Dinerstein, H. L. 1983, *Ap. J.* (*Letters*), **271**, L13.
Sivan, J. P. 1974, *Astr. Ap. Suppl.*, **16**, 163.
Solomon, P., Rivolo, A. R., Mooney, T. J., Barret, J. W., and Sage, L. J. 1987, *Star Formation in Galaxies*, ed. C. J. Lonsdale Persson (Washington: GPO).
Stark, A. A., Bally, J., Linke, R. A., and Heiles, C. 1987, in preparation.
Terebey, S., and Fich, M. 1986, *Ap. J.* (*Letters*), **309**, L73.
Weaver, H., and Williams, D. R. W. 1973, *Astr. Ap. Suppl.*, **8**, 1.
Weiland, J. L., Blitz, L., Dwek, E., Hauser, M. G., Magnani, L., and Rickard, L. J. 1986, *Ap. J.* (*Letters*), **306**, L101.

F. BOULANGER: Infrared and Processing Analysis Center, Caltech 100–22, Pasadena, CA 91125

M. PÉRAULT: Radio-Astronomie, Ecole Normale Supérieure, 24 rue Lhomond, 75231 Paris Cedex 05, France